

TWO-DEGREE-OF-FREEDOM PLAFORM AS A TOOL FOR COOPERATION BETWEEN MOBILE ROBOTS AND UAVs

Emerson Kazuyoshi Kaneda - 61103

Dissertation presented to the School of Technology and Management of Bragança to
obtain the Master Degree in Industrial Engineering.

Work oriented by:

Prof. Dr. José Luís Sousa de Magalhães Lima

Prof. Dr. Flávio Luiz Rossini

Prof. Dr. Marcio Rodrigues da Cunha

Bragança

2024



INSTITUTO POLITÉCNICO Escola Superior
DE BRAGANÇA de Tecnologia e Gestão

TWO-DEGREE-OF-FREEDOM PLAFORM AS A TOOL FOR COOPERATION BETWEEN MOBILE ROBOTS AND UAVs

Emerson Kazuyoshi Kaneda - 61103

Dissertation presented to the School of Technology and Management of Bragança to
obtain the Master Degree in Industrial Engineering.

Work oriented by:

Prof. Dr. José Luís Sousa de Magalhães Lima

Prof. Dr. Flávio Luiz Rossini

Prof. Dr. Marcio Rodrigues da Cunha

Bragança

2024

Dedication

To my family, for all the support and encouragement to face life's challenges. Both those who follow my journey on a daily basis and those who are eternalized in my memories.

To my friends who shared the experience of living in another country. During my time in Portugal, I met a number of incredible people who will live on in my memories forever as wonderful experiences.

To my university friends, once eternalized as "Survivors of Electronics", and to everyone who walked the academic journey alongside me.

To my teachers at the Federal Technological University of Paraná for all the curricular and extra-curricular learning I've done.

To my colleagues at CeDRI as my mentors during the development of this work.

Acknowledgement

I would like to thank the Federal Technological University of Paraná and the Polytechnic Institute of Bragança for the opportunity to carry out this work. This work is a partnership between the two institutions due to the double degree agreement, which is an excellent opportunity for students from both institutions in their academic careers.

I also would like to thank the Intelligent Robotics Digitization Center (CeDRI) for guiding me in the development of this work

Abstract

Unmanned Ground Vehicle (UGV) and Unmanned Aerial Vehicle (UAV) represent a large relevance in the current technological context, enabling its application in different areas of knowledge. The approach should be developed and applied to operations by UAV of small size, whether applied indoors or outdoors. During the present work a self-leveling platform prototype will be built that allows a drone to be landed on horizontal surface regardless of the angle of its support.

The main objective of this work is to study the Kinematics behavior of a self-leveling platform dedicated to cooperative operations between robotic systems heterogeneous. In this sense, both the development of the control system and hardware will be developed and validated in different environments, such as regular terrain and irregular.

Keywords: Robots; Control; Self-Leveling platform; cooperation

Resumo

Os Veículos Terrestres Não Tripulados (VTNT) e os Veículo Aéreo Não Tripulado (VANT) representam uma grande relevância no contexto tecnológico atual, possibilitando sua aplicação em diferentes áreas do conhecimento. A abordagem deve ser desenvolvida e aplicada em operações de VANT de pequeno porte, seja em ambientes internos ou externos. Durante o presente trabalho será construído um protótipo de plataforma autonivelante que permite a aterragem de um drone em superfície horizontal independentemente do ângulo do seu suporte.

O principal objetivo deste trabalho é estudar o comportamento cinemático de uma plataforma autonivelante dedicada a operações cooperativas entre sistemas robóticos heterogéneos. Neste sentido, tanto o desenvolvimento do sistema de controlo como o hardware serão desenvolvidos e validados em diferentes ambientes, tais como terrenos regulares e irregulares.

Keywords: Robótica; Controle; Plataforma de auto-nivelamento; cooperação

Contents

Acknowledgement	vii
Abstract	ix
Resumo	xi
Acronyms	xxi
1 Introduction	1
1.1 Background	4
1.2 Objectives	6
1.3 Thesis structure	7
2 State of art and Study of tools	9
2.1 Structure of the platform	10
2.1.1 Gimbaled Platform	13
2.1.2 Bidirectional platform	14
2.1.3 Delta Platform	16
2.1.4 Stewart Platform	17
2.2 Actuators	19
2.2.1 DC Motor	19
2.2.2 Servo Motor	20
2.2.3 Step motor	21

2.2.4	Linear Actuators	22
2.3	Inertial Measurement Unit (IMU)	23
2.3.1	Accelerometer	23
2.3.2	Gyroscope	24
2.4	Hardware	25
2.5	Controllers	27
2.5.1	PID controller	28
3	System methodology	31
3.1	Physical construction of the platform prototype	31
3.2	Kinematics Analysis of the platform	32
3.3	Hardware Assembly	33
3.4	Software development	34
3.5	Test and Validation	35
4	Development	37
4.1	Physical Structure	37
4.2	Hardware Implementation	42
4.3	Software Implementation	44
4.3.1	Measuring Data and Calculating Angles	45
4.3.2	PID Development	47
4.3.3	Data Transmit	48
5	Results	51
5.1	Kinematic Validation measuring the angles	51
5.2	Controller Validation	56
5.2.1	P gain	57
5.2.2	D gain	59
5.2.3	I gain	59
5.3	Dynamic test using weights	64

5.4	Environment test intend to couple in a mobile robot	66
5.4.1	Indoor Tests	67
5.4.2	Outdoor Tests	68
5.4.3	Take off and Landing Operations of an drone	70
6	Conclusion and Future Work	71
A	Proposta Original do Projeto	81
B	Outro(s) Apêndice(s)	84

List of Tables

1.1	Relation of % of slope and degree [17]	5
2.1	PID Tuning Parameters [52]	30
3.1	Hardware Components List	34
4.1	Lengths of structure parts	40
5.1	Maximum and Minimum angles	55
5.2	Errors	56
5.3	Indoor Test Errors	67
5.4	Outdoor Test Errors	69
5.5	Indoor Test Errors	70

List of Figures

1.1	Review of platforms type[12]	2
1.2	Iberian Relief Map	4
1.3	Slope map of Bragança city	5
1.4	Cronogram in Gantt Graph	7
2.1	Cooperation of UAV-UGV in precision land operation [8]	10
2.2	Mobile Manipulator with a 2 DoF self stabilizer platform [3]	11
2.3	Roll Pitch and Yaw angles on aircraft [22]	12
2.4	Gimbaled Structure [19]	13
2.5	Reference Axis of the Gimbaled Structure [19]	14
2.6	Ball on Plate system [24]	15
2.7	Layout of the actuator [25]	16
2.8	Delta platform parallel robot [28]	17
2.9	Stewart Platform example [29]	18
2.10	Stewart Platform on mobile robot for self stabilization [30]	18
2.11	DC motor with encoder [31]	19
2.12	Signal to control an servo motor [33]	20
2.13	Full Step configuration [34]	21
2.14	Micro-Steps Configuration [34]	22
2.15	Commercial Linear Actuator with 100mm length [36]	22
2.16	Control Diagram Topology [50]	27
3.1	3D model of platform	32

3.2 Block Diagram of the system	34
4.1 Mechanical parts printed using Polylactic Acid (PLA) filament	38
4.2 Universal Joint	39
4.3 Physical platform with reference	39
4.4 Frontal view of the platform [25]	40
4.5 Lateral view of the platform	41
4.6 Slope function	42
4.7 Circuit Schematic	43
4.8 Flowchart of data travel	45
4.9 Control Diagram	45
5.1 Drone over the platform	52
5.2 Angled Level Meter	52
5.3 How measured the angles	53
5.4 Pitch Angle Calibration	53
5.5 Roll Angle Calibration	54
5.6 Correct Pitch Kinematic	55
5.7 Correct Roll Kinematic	55
5.8 Proportional Gain (Kp) equals 0.1	57
5.9 Kp equals 0.2	57
5.10 Kp equals 0.3	58
5.11 Kp equals 0.4	58
5.12 Kp equals 0.5	59
5.13 Derivative Gain (Kd) equals 0.1	60
5.14 Kd equals 0.2	60
5.15 Kd equals 0.3	61
5.16 Kd equals 0.4	61
5.17 Integral Gain (Ki) equals 0.005	62
5.18 Ki equals 0.01	62

5.19 Ki equals 0.05	63
5.20 Ki equals 0.1	63
5.21 Step response with 1kilogram (kg) load	64
5.22 Step response with 2kg load	65
5.23 Step response with 3kg load	65
5.24 Step response with 4kg load	66
5.25 Example of Indoor and Outdoor tests	67
5.26 Self-Leveling in Indoor Test	68
5.27 First Outdoor Test	68
5.28 Second Outdoor Test	69
5.29 drone landing	70

Acronyms

μs microseconds.

3D Three Dimensional.

AT commands Comandos Hayes Commands.

BLE Bluetooth Low Energy.

bps bits per second.

DIP Dual In-line Package.

DoF Degree of Freedom.

Hz Hertz.

I2C Inter-Integrated Circuit.

IMU Inertial Measurement Unit.

IoT Internet of Things.

Kd Derivative Gain.

kg kilogram.

Ki Integral Gain.

K_p Proportional Gain.

LSB Least Significant Bit.

MAE Mean Absolute Error.

ME Mean Error.

MEMS micro-electromechanical systems.

mm millimeter.

ms milliseconds.

MSB Most Significant Bit.

OS Operational System.

P Proportional.

PCB Printed Circuit Board.

PD Proportional and Derivative.

PIC Peripheral Interface Microcontroller.

PID Proportional, Integral and Derivative.

PLA Polylactic Acid.

PVC Polyvinyl Chloride.

PWM Pulse-Width Modulation.

RMSE Root Mean Squared Error.

RPM Rotation Per Minute.

SCL Serial Clock.

SDA Serial Data.

SPI Serial Peripheral Interface.

UART Universal Asynchronous Receiver/Transmitter.

UAV Unmanned Aerial Vehicle.

UGV Unmanned Ground Vehicle.

VANT Veículo Aéreo Não Tripulado.

VTNT Veículos Terrestres Não Tripulados.

VTOL Vertical Take-Off and Landing.

Wi-Fi Wireless Fidelity.

Chapter 1

Introduction

Cooperative robotics has been increasingly applied in industry, agriculture [1] [2] [3] [4], mapping [5] [6], and even in public safety [7]. One of cooperation that has been developed is the precision landing of UAV on UGV mobile platforms [8] [9], whether to complete its operation or to change batteries with a hot swap technique so that it can extend its mission due to the high battery consumption required by UAV. Another field that being developed is the use of manipulators on mobile robots [3] [10] [11], these already have purposes such as pick-and-place operations or collect objects in factories, also harvest fruits in farms.

In those cases, the mobile robot UGV has a fundamental role since it is the basis for the operations of other robots, especially in outdoor operations, for UAV they need to perform a precision landing on an ideally stabilized ground horizontally for not fall down due the self weight, in the case of manipulators the importance of a stabilized base is greater, because the kinematics of these robots are dependent of origin point as a reference.

The work of [12] is a review of many types of platforms, since the fixed docking station to mobile platforms, in this review 2 types of platforms used to cooperate with UAV are a fixed platform with self leveling for landing operations on irregular grounds, and the other is a mobile land platform, the idea of a self leveling platform intended to mount in a mobile robot is the main propose of this present work. The Figure 1.1 shown the

platforms cited in the work of [12], the Figure 1.1a present the self leveling platform and the Figure 1.1b exhibit a mobile land platform cooperating with a UAV.



(a) Self Leveling Platform



(b) Mobile Platform cooperating with UAV

Figure 1.1: Review of platforms type[12]

However, the operability of robots is still limited for certain environments, except the industries that has a fully designed and controlled internal environment so that the factory operates as designed. According with Bearing News exist some infrastructure that are not adopted such as uneven surfaces and slopes, the author show in the news a robot with mechanic self-stabilizer to solve this problems [13], on the other hand this robot have only 1 Degree of Freedom (DoF) and the focus of this robot is operation in flatter cities.

Another interesting type of application for mobile self-leveling platforms, is in the cooperation of other static robots, like manipulators or automated dock stations for UAV. About manipulators the mobile self-leveling platforms enable a robotic arm to operate in irregular places that change abruptly the origin position of the robot, the main objective of this stabilization is generate a smooth moving on the origin position of the manipulator. Further in dock stations, the main problem in missions using UAV is the low battery capacity and land in regular grounds, a technique for solve the battery problem is the hot swap, this technique is based in change the battery without turn off the UAV system. So

combining the two problems and solutions, a mobile self-leveling platform coupled with a hot swap dock station can be a solution to extend the time of the operations of UAV. This solution is composed with many components, that can separate in the following parts:

- Mobile Robot
- Self-Leveling Platform
- Hot Swap Dock Station
- UAV

The present work is focused in the development of the Self-Leveling Platform only, however the project was minded with intended to couple the platform over a mobile robot and below of an dock station to cooperate in missions and tasks.

The platform's inclination angle depends on the environments the robot will be exposed to. Considering the topography of the Iberian peninsula, that is the main environment the platform is exposed, it's evident that a UGV would encounter mountainous landscapes, as it can be observed in the Figure 1.2

how we see in the Figure 1.2, the Iberian territories is basically composed by highlands rounded by mountains [14], also it's possible see the color gradient becomes from 100 meters to 1000 meters indicating a high slope. That information is important to develop an outdoor mobile platform to consider the maximum slope the robot can reach, in the case of a cooperation between UAV and UGV if the platform can't stabilize due the maximum inclination is lower than the ground slope the robot have less area to operate.

According to Sánchez-Martínez in traditional olive farms, the trees grown in terrains with 20% of slope, making it difficult to mechanize the harvest and irrigation [15].

Based on this problems, this present work propose the development of a Cooperative 2 DoF Self-Stabilize Platform Intended to couple on a mobile robot. To construct this

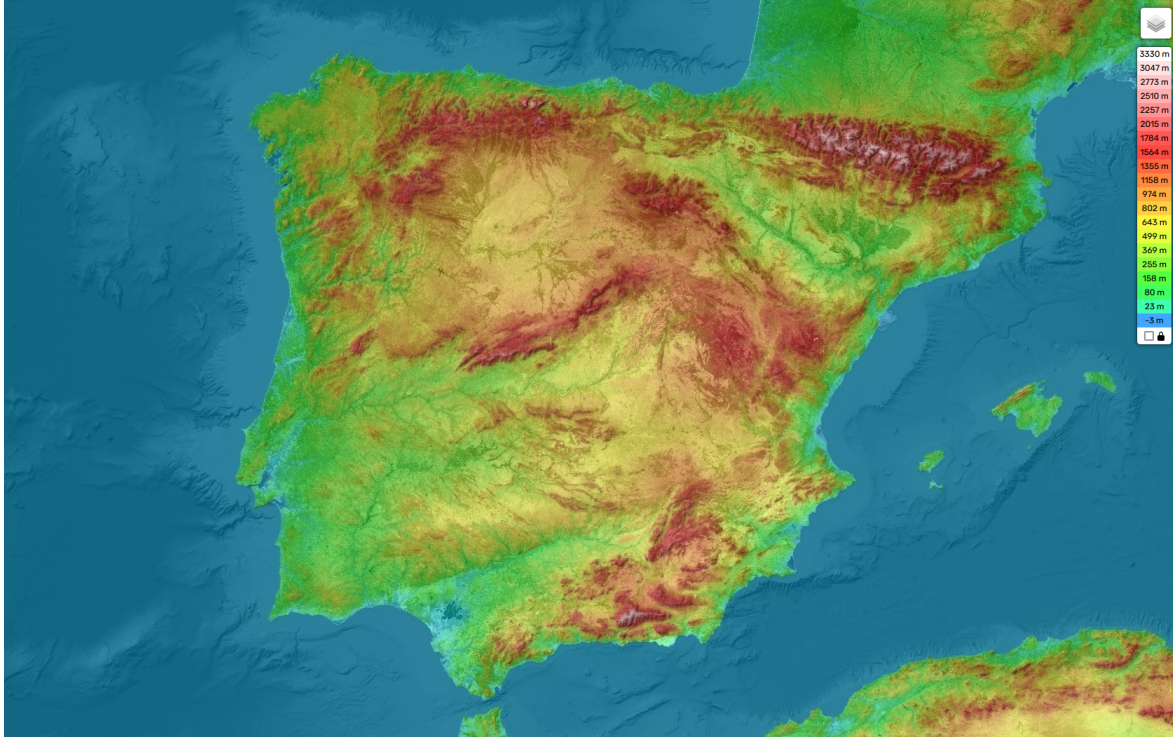


Figure 1.2: Iberian Relief Map

project, a study with Proportional (P), Proportional and Derivative (PD) and Proportional, Integral and Derivative (PID) controller was projected to analyze the best stabilization of the slope for each direction, to measure and close the loop control a Inertial Measurement Unit (IMU) sensor was used.

1.1 Background

To facilitate the use of mobile robots and their cooperation with other robots, the development of a landing platform that adapts to uneven terrain allows better cooperation between the two robots.

Based on this, the self-stabilizing platform will be the focus of this work aiming at the development of mobile robots for the purpose of landing platforms, however with the possibility of expanding this work to improve a general purpose platform.

The test environment will be considered the slope of the city of Bragança, taking into

account the map created in Gonçalves [16] work, as we can see below.

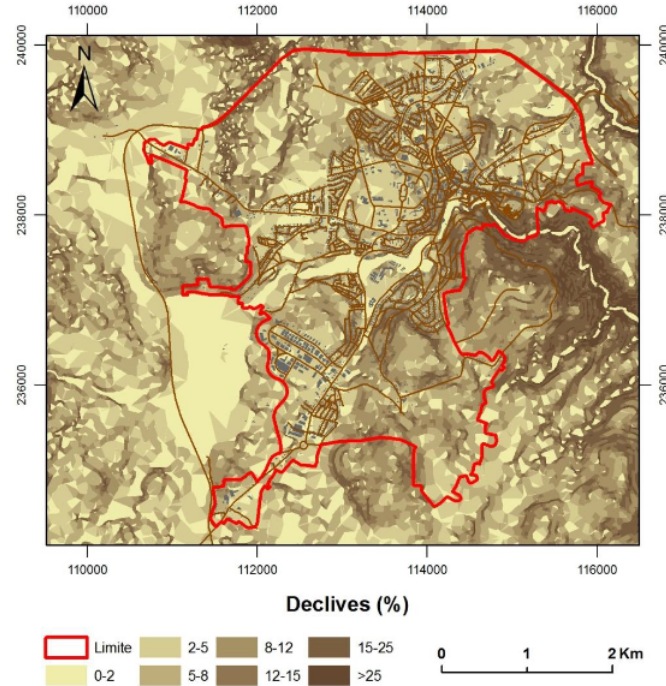


Figure 1.3: Slope map of Bragança city

The relation of degrees to % of slopes follow the table 1.1

Slope (%)	Degrees
0 à 2	0 à 1.15
2 à 5	1.15 à 2.86
5 à 8	2.86 à 4.57
8 à 12	4.57 à 6.84
12 à 15	6.84 à 8.53
15 à 25	8.53 à 14.03
> 25	> 14.036

Table 1.1: Relation of % of slope and degree [17]

For this city have many uneven places, of course a mobile robot can not operate over acclivity grounds, on the other hand, in most urban areas, streets and green areas it has a considerable slope that makes it possible to move a mobile robot but makes it impossible to land a UAV.

The heterogeneity of robots plays a crucial role in executing tasks, especially in complex scenarios such as precision land operations. By combining robots with different functionalities and capabilities, it is possible to distribute tasks more efficiently, allowing each robot to contribute its specific skills. This diversity not only improves the group's efficiency, but also makes it easier to adapt to different situations and challenges that may arise during the mission. The research of [18] shows that variation in robot capabilities can lead to superior collective performance, as collaboration between agents with complementary skills results in a more robust and effective approach to carrying out complex tasks.

How the focus is the development of robot heterogeneity in advent missions between UAV and UGV, the present work is dedicated to the development of a landing platform as a component of a mobile robot for cooperation in precision landings of aerial robots.

1.2 Objectives

The main objective of this present work is develop a prototype of the platform itself, according to the following features.

The platform must reach at least a maximum of 15 degrees and a minimum of -15 degrees of inclination on each axis, or have a platform positioning range of up to 30°. In addition, the response to this tilt must be fast, the stabilization time must be less than or close to 1 second.

The landing area is focused to support an hexacopter and smaller drones, so the plate would have at least 500 millimeter (mm) of length and 500 mm of width. However for the structure support heavy drones it depends the type of structure and the resource available to design the platform with strong materials, thus the minimum weight that the platform of the present work must support is 3 kg.

Hardware, software and control system development need to be validate in different environments, also the kinematics behavior need to be studied and validate in regular and irregular grounds.

The development schedule for this work follows the Gantt graph below in Figure 1.4

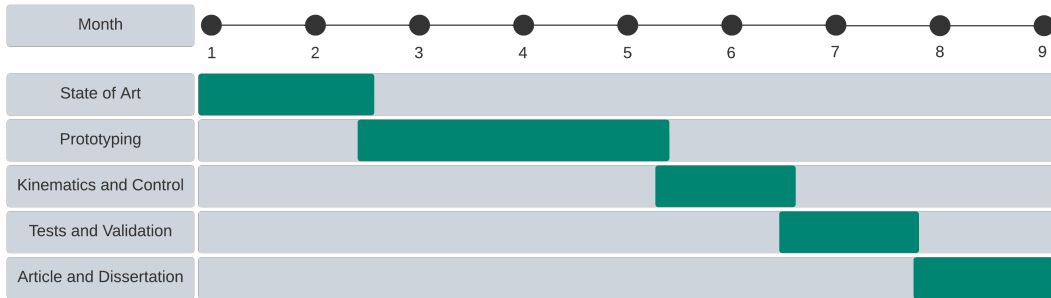


Figure 1.4: Cronogram in Gantt Graph

1.3 Thesis structure

This thesis is structured in introduction, state of the art, methodology, development, results and finally conclusion and future work.

The introduction contextualizes the study on the cooperation and heterogeneity of robots in their operations, exposing the main problem in cooperation between UAV and UGV in outdoor environments. At the end, there is the background to the work carried out and the intended objectives to be achieved at the end of the development.

The state of the art includes a review of the literature on the types of mobile platforms developed in other works, and some types of platform that can be coupled to a mobile robot. There is also a review of the basic components used in the development of existing work, the sensors used and the classic PID controller.

The methodology describes the order of the platform's development process, including the mechanical part and its kinematics, the electronic part showing the components used in the implemented system, and finally the flow of data in the software processed by the computer system.

The development describes the mechanical assembly process, kinematic calculations, sensor reading and signal filtering, pitch and roll angle calculations, calculation of some PID parameters and how data sampling was carried out along with interaction with the

platform.

The results section shows the behavior of the platform under some possible scenarios that it may be subjected to, these scenarios being the response to the step without load, with loads of up to 5 kg and under some vehicle simulating a mobile robot.

Finally, the last chapter is the conclusion of the work carried out, containing the points of error and success and analysis for future work.

Chapter 2

State of art and Study of tools

In the field of mobile robotics, cooperation between them has been gaining ground in scientific and engineering research, many applications of cooperative robots can be implemented both for agriculture [3], public safety [7] and mapping [5] [6]. Some works are focus in the cooperation of UGV and UAV [19], and for this cooperation one interaction of both robots are the precision planning with a mobile platform.

Self-stabilizer platforms have many applications like carries heavy loads without drop them, in the work of [20] was developed a mobile robot with a self-stabilizer platform to go up or down stairs with heavy loads over the platform. This platform was developed with 2 DOF allowing better stabilization when climbing while performing cornering maneuvers

The work of [19] have a mobile robot with a stabilizer platform based on a Gimbal mechanism to provide a base for Vertical Take-Off and Landing (VTOL), this work model the grounded robot developed for academic uses ATRV-Jr in 3D to execute some simulations. The simulations of this cooperation show a significant increase in the range operation of the VTOL. On the other hand the structure limits the maximum weight of the payload, for heavy drones like an professional hexacopter this structure is not suitable.

Figure 2.1 shows the idea of a mobile land platform without a self leveling, the work of [8] result in a extension of the range operation of the UAV.

In the work of [3] the mobile robot use a similar 2 DOF gimbled self-stabilizer platform, however carries on the platform a manipulator robot that need the XY -plane as a static

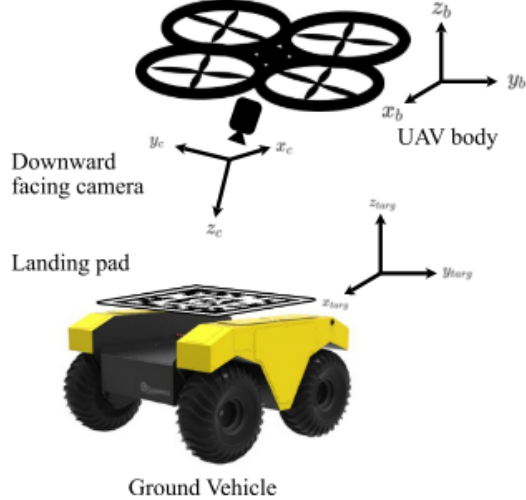


Figure 2.1: Cooperation of UAV-UGV in precision land operation [8]

reference so that the kinematics do not suffer with the irregularities in the ground.

Other interesting cooperation with a mobile platform is a mobile manipulator, to harvest banana [3] propose a mobile platform with 2 DoF stabilizer to cooperate with a manipulator, the Figure 2.2.

To develop this platforms some characteristics need consider in the construction of the robot. That are the follow features:

- Structure of the platform
- Actuators
- Sensors
- Hardware
- Controller

2.1 Structure of the platform

About the type of structure, this feature is the most important to decide many components and the behavior of the platform, the most common type of structure are 4 as listed below,

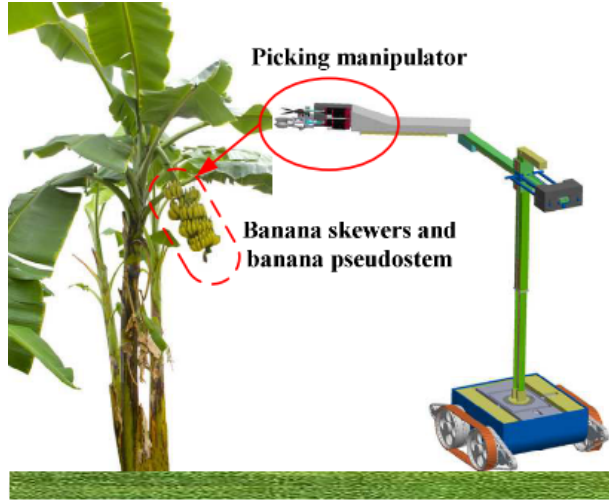


Figure 2.2: Mobile Manipulator with a 2 DoF self stabilizer platform [3]

each have your kinematic and dynamic behaviors.

- Gimbaled Platform
- Bidirectional platform
- Delta platform
- Stewart platform

To analyze this structures the main features are the kinematic complexity and how much cost to develop those structures.

The kinematics of the platform leveling is based on the Euler angles with the aircraft principal axis names, Roll, Pitch and Yaw angles [21]. As it is visible in the Figure 2.3, those angles is related with one of three Cartesian axis, and are the least necessary to reach all positions for navigate in the space.

It is also visible in the Figure 2.3 the reference of the air craft is in the middle of it, in a self-leveling platform the reference point is the center of the plate.

The kinematics analysis for this angles follow the rotation matrix of them, the matrix of equations 2.1, 2.2 and 2.3 are the rotation matrix of Roll, Pitch and Yaw angles, respectively [23].

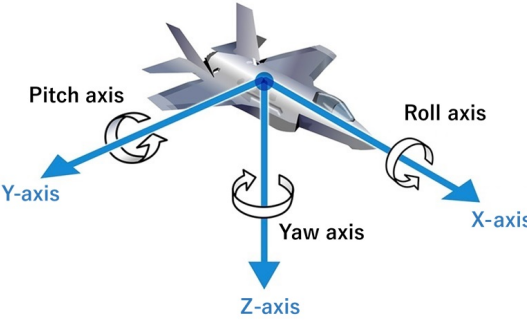


Figure 2.3: Roll Pitch and Yaw angles on aircraft [22]

$$R(\theta) = \begin{bmatrix} 1 & 0 & 0 \\ 0 & \cos(\theta) & -\sin(\theta) \\ 0 & \sin(\theta) & \cos(\theta) \end{bmatrix} \quad (2.1)$$

$$P(\theta) = \begin{bmatrix} \cos(\theta) & 0 & \sin(\theta) \\ 0 & 1 & 0 \\ -\sin(\theta) & 0 & \cos(\theta) \end{bmatrix} \quad (2.2)$$

$$Y(\theta) = \begin{bmatrix} \cos(\theta) & -\sin(\theta) & 0 \\ \sin(\theta) & \cos(\theta) & 0 \\ 0 & 0 & 1 \end{bmatrix} \quad (2.3)$$

The Cartesian coordinates vector can be rotated with the following transformation 2.4, generating a new point in space.

$$V'_{xyz} = Y(\theta) \cdot P(\theta) \cdot R(\theta) \cdot V_{xyz} \quad (2.4)$$

In sequence are a review of each type of platform and yours positives and negatives features considering the development of an mobile platform using a self-stabilizer platform coupled to cooperate with another robots.

2.1.1 Gimbaled Platform

A Gimbaled Structure is composed with the same concept used in the products to stabilize phone cameras. This structure have 2 DoF, one for stabilize the slope and other to rotate the plane of interest. The Figure 2.4 shown a prototype of a Gimbaled structure for stabilize an platform, it is visible a camera on the structure used for sensor to close the loop control.



Figure 2.4: Gimbaled Structure [19]

The work of [19] used a mobile Gimbaled platform to cooperate with an VTOL, the payload on the platform have 5.8 kg, this payload was a VTOL model Thunder Tiger Raptor 90SE, and this model have a endurance flight time of 18 minutes. This work has demonstrated the 2 DoF Gimbaled Structure is proven to be adequate for ensuring a horizontal landing platform for VTOL. And increase significantly the range of the operation of an UAV.

The kinematic of this structure according to [19] is based on 2 axis, the Elevation Axis and the Heading, as the Figure 2.5 demonstrate those reference axis.

According to the author, the kinematic of this platform is based on the Elevation vector and Heading vector, those two are rotated following the Z and Y axis reference of the platform, as described by 2.5 and 2.6.

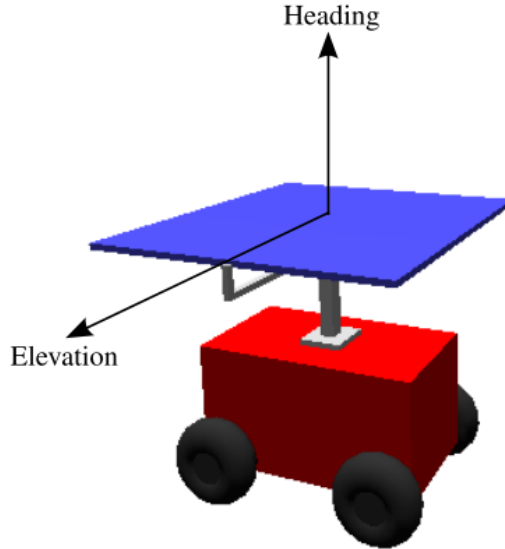


Figure 2.5: Reference Axis of the Gimbaled Structure [19]

$$V'_{el} = Y(\theta) \cdot V_{el} \quad (2.5)$$

$$V'_{hd} = P(\theta) \cdot V_{hd} \quad (2.6)$$

so a Gimbaled platform has simple kinematics that are based around the Pitch and Yaw angles, requiring only 2 DoF.

2.1.2 Bidirectional platform

A bidirectional platform typically refers to a robotic or mechanical system capable of moving along two independent axes. These platforms often consist of a base that supports a moving part, which can be manipulated along two perpendicular directions (usually referred to as the X and Y axes). The movement can be linear, rotational, or a combination of both, depending on the specific application requirements. The primary purpose of such platforms is to provide precise positioning and orientation capabilities in environments where high precision and repeatability are critical.

This type consists in the movement along the Y and X axis, so the main angles in

this platform are the Roll and Pitch, different by the Gimbaled that use Pitch and Yaw. A Bidirectional platform also have 2 DoF but can use 2 or 4 motors to generate more torque and support heavy loads, on the other hand to use 4 motors a synchronization of the motors in the same axis need to be precise. In general these platform have a central support to complete 3 point of the plane, in Figure 2.6 is visible a support under the platform, this point is the reference point for rotation of the angles Roll and Pitch.

The most common application for bidirectional platform is the ball balancing, where the platform move the ball to the center or to the set point position and keep the ball stabilized on the position, this can be seen in the Figure 2.6.

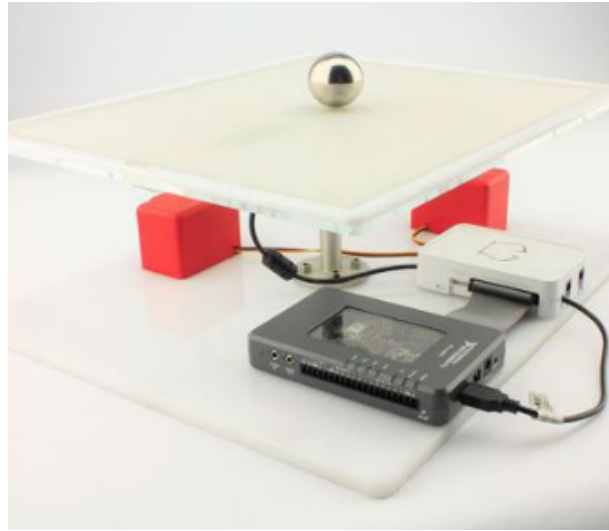


Figure 2.6: Ball on Plate system [24]

The kinematics of the bidirectional platform is based on the layout of the brackets coupled on the actuator and the distance between the motor and the center of the platform [25], in the Figure 2.7 have a simple layout of the actuator of the platform

Each layout have different equations for kinematics, but the rotation is over the same angles pitch and roll.

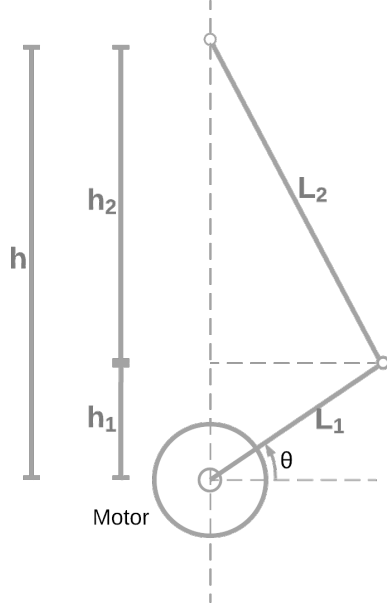


Figure 2.7: Layout of the actuator [25]

2.1.3 Delta Platform

The Delta robot is a parallel robot which was invented in the early 1980s by Reymond Clavel [26]. A primary application of the Delta Robot is pick and place operation and hence it is characterized by speed and accuracy . The steeper of a delta robot consists of a base and an end effector which is mechanically interconnected through links and a base corresponds to a non-revolute joint. Due to this design, the moving mass is minimized, and therefore Delta robots are popular for packaging, medical and other applications where low cost and high speed movement and accuracy are required [27].

A Delta platform have 3 DoF, how this platform have 3 point due each actuator, this type do not have a central support, and that means the reference point for the platform rotation is mobile, this can raise or lower the platform depending to the length and layout of the actuators.

The advantage of this platform how was cited before is the ability to support more load due to its structure, on the other hand the kinematics become more complex due to the increase in DoF.

In the work of [28] the author talk about the kinematics of the platform based on the Figure 2.8, were it is clear to see the 3 DoF. The author of [28] demonstrate the forward and inverse kinematics using the rotation matrix using the center of the platform as reference, in the Figure 2.8 this point is represented as "x,y,z" point.

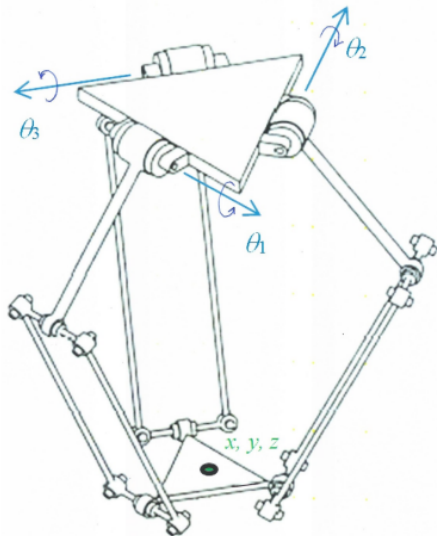


Figure 2.8: Delta platform parallel robot [28]

Williams trace many trajectories using a analytic solution for the kinematic of the delta platform. The author also say the solution is not trivial, this is a important consideration in the project of an self-leveling platform, due the complexity of the kinematics[28].

2.1.4 Stewart Platform

The Stewart platform, also known as a parallel manipulator or hexapod, is a type of robot characterized by its closed-loop kinematic chain, where six prismatic or rotary actuators control the movement of a single platform. Introduced by D. Stewart in 1965 for use as a flight simulator, the Stewart platform has since become a critical element in numerous applications requiring precision motion, high stiffness, and load-bearing capacity [29].

Due to its unique characteristics, the Stewart platform is used in applications ranging from flight simulators, telescope alignment, and satellite antenna positioning to surgical

robots and advanced manufacturing systems. The high load capacity, accuracy, and rigidity make it suitable for these precision-demanding tasks. Moreover, its compact design with all actuators positioned close to the base provides greater stability and control[29]. In the Figure 2.9 show an example of Stewart Platform, it is possible to see the platform have 6 DoF, increasing the complexity of the kinematics.



Figure 2.9: Stewart Platform example [29]

The ability to use a Stewart platform in mobile robots has been studied as a good stabilization option due to its behavior and characteristics. In the Figure 2.10 show an work on the application of a Stewart platform coupled on a mobile robot for self stabilization [30].



Figure 2.10: Stewart Platform on mobile robot for self stabilization [30]

This work analyze the kinematics of the platform over the mobile robot, on the other hand the the robot need more advanced controllers for the actuators [30].

2.2 Actuators

Actuators are crucial components in robotic platforms, providing the mechanical motion necessary for tasks such as positioning, navigation, manipulation, and more. The choice of actuator significantly influences a robot's performance, efficiency, and versatility. The most commonly used actuators in constructing robotic platforms include servo motors, stepper motors, and linear motors. This review discusses the characteristics, advantages and disadvantages of these actuators in robotics.

2.2.1 DC Motor

DC motors are widely used in robotics for applications requiring simple, continuous rotation. These motors convert direct current electrical energy into mechanical energy through the interaction of magnetic fields generated by the motor's internal winding's and the external magnetic field.

The main advantage is the high torque and the simplicity usage as a basic electric component, on the other hand the main disadvantage is the limited precision, to control the position the DC motor need an encoder to close a loop control [31].

The DC motor with incremental encoder is the most common type used in applications that need position control, on the other hand this type of encoder accumulate a small error in permanent regime, the Figure 2.11 shows a example of this type of motor with an incremental encoder module coupled.



Figure 2.11: DC motor with encoder [31]

Other DC motor used in robots which need a high position precision throughout time is the DC motor with absolute encoder, this type return the exactly position of the motor with a despicable error, so in permanent regime the error on position is despicable or do not exist.

2.2.2 Servo Motor

Servo motors are rotary or linear actuators that enable precise control of angular or linear position, velocity, and acceleration. A servo motor is typically composed of a motor coupled to a sensor (like an encoder) for feedback, and a controller to adjust the motor's output based on feedback signals.

A simple control of an servo motor is show in Figure 2.12, the position of the servo follows a proportional resolution of the duty cycle of Pulse-Width Modulation (PWM), were 1 milliseconds (ms) of high signal equals to minimal angle and 2 ms equals the maximum angle, this maximum and minimum can be 0 to 180 degrees or -90 to 90 degrees [32].

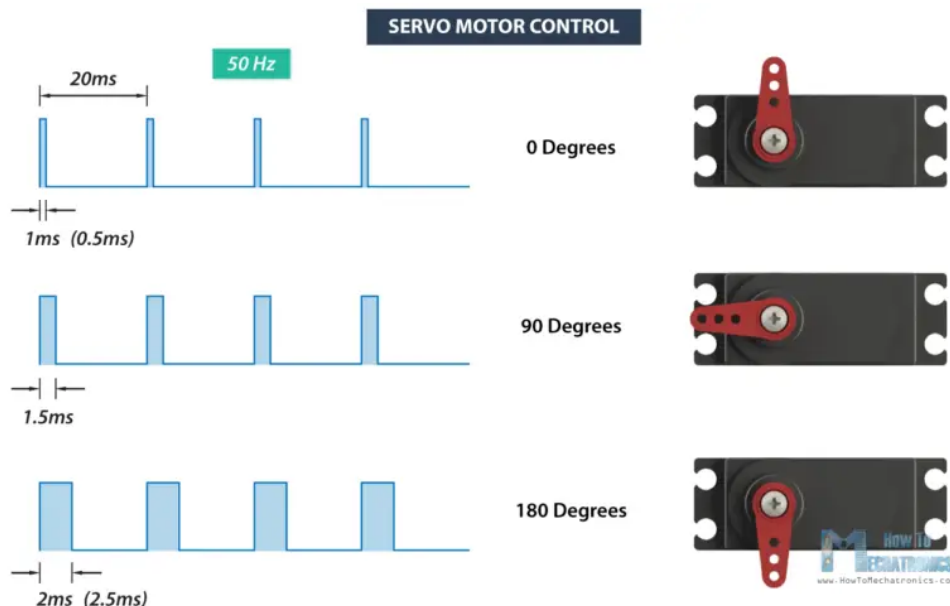


Figure 2.12: Signal to control an servo motor [33]

Since this motor have a position closed loop control, this motor is severely considered

in many projects for manipulators and other robots [29], on the other hand this type of motor need a control more complex than the others.

2.2.3 Step motor

Stepper motors are electric motors that move in discrete steps, making them suitable for applications requiring precise position control without feedback. They operate in open-loop control systems, where each pulse sent to the motor corresponds to a specific angle of rotation. This motor is simpler to control and less expensive than servo motors, as they do not require a feedback mechanism.

For position control this motor is a good option due to the movement of the angle in discrete steps, however for high speed this motor requires more effort to generate high torque, thus being a limiting characteristic in a robotics project. But this feature can easily solve using reduction gear boxes.

The reason for the high precision in position control of this type of motor is due the principal work of the inside the motor, the rotor and stator are composed of permanent magnets and coils, when a current circulates through the coils a magnetic field is generated attracting one of the magnetic poles of the magnet, consequently when switching the flux between the coils a circular movement is generated in the rotor in order to rotate the desired axis [34].

In the Figure 2.13 the author show the full step configuration, also have the micro-steps for this type of motor that increase the precision of the position, the Figure 2.14 shows the example of micro-step configuration.

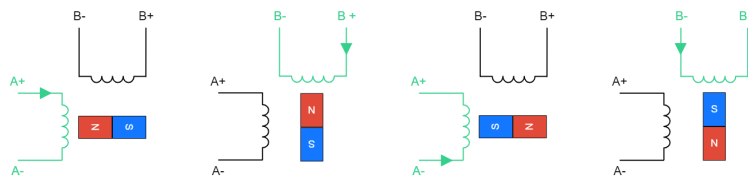


Figure 2.13: Full Step configuration [34]

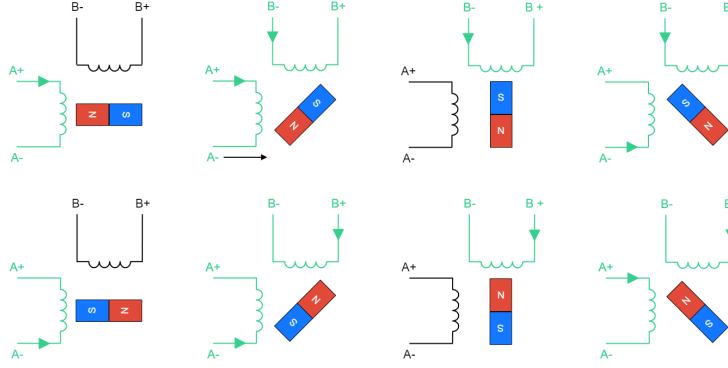


Figure 2.14: Micro-Steps Configuration [34]

2.2.4 Linear Actuators

An electric linear actuator is a common device used to create motion. It consists of three main parts: a spindle, motor, and gears. The motor, which can be either AC or DC depending on the power needed, transforms electrical energy into mechanical energy when activated by a simple control, like pressing a button. This energy drives the gears, turning the spindle, which moves the piston rod in or out [35].

The Figure 2.15 show an commercial example of linear actuator, this type also can be named prismatic joint, due the joint type of robots [29].



Figure 2.15: Commercial Linear Actuator with 100mm length [36]

Generally, a spindle with more threads moves slower but can handle heavier loads, while fewer threads allow for faster movement but can carry less weight [35].

However the disadvantages of linear actuators is the high cost compared to traditional rotary motors due to their specialized design and materials. Another disadvantage is the limited range of the movement, due the length of the motor track [29].

2.3 Inertial Measurement Unit (IMU)

An Inertial Measurement Unit is a type of sensor used to measure an object's acceleration, angular rate, and sometimes magnetic field. It plays a crucial role in navigation systems, robotics, drones, smartphones, and many other applications where motion and orientation are of concern. IMUs typically consist of a combination of accelerometers, gyroscopes, and sometimes magnetometers [37].

The IMU works by using the combined data from its accelerometers and gyroscopes to calculate the object's current orientation and motion. The accelerometer provides a measure of the device's linear motion, while the gyroscope provides information about how the device is rotating. Some IMUs also use magnetometers to correct for drift in the gyroscope and provide a more stable and accurate orientation.

IMUs are commonly used in systems that need to maintain an awareness of orientation and movement, such as drones for stabilizing flight, robots for motion control, and smartphones for features like screen rotation and step tracking.

2.3.1 Acelerometer

An accelerometer is a sensor that measures the acceleration experienced by an object. It provides data along three orthogonal axes: X, Y, and Z. This data can be used to determine the direction and magnitude of gravitational forces acting on the object, which allows us to estimate its orientation in space. The sensor detects acceleration forces, which can include both the static force of gravity and the dynamic forces caused by motion. When an object is at rest or moving at a constant velocity, the accelerometer

senses only the static acceleration due to gravity, which helps in determining the tilt or orientation of the object [37] [38].

The raw data from an accelerometer are typically three values corresponding to the acceleration in the X, Y, and Z axes (denoted as Ax, Ay, and Az). By analyzing the acceleration due to gravity along these axes, it is possible to calculate the pitch and roll angles, which describe the tilt of the object relative to the ground [37].

The main data calculated with this sensor is the Pitch and Roll, they are the two primary angles that define the orientation of an object with respect to the Earth's gravity. Here's how to calculate them from the accelerometer data as following 2.7 and 2.8 [25]:

$$Pitch = \arctan\left(\frac{A_y}{\sqrt{A_x^2 + A_z^2}}\right) \quad (2.7)$$

$$Roll = \arctan\left(\frac{-A_x}{A_z}\right) \quad (2.8)$$

2.3.2 Gyroscope

A gyroscope is a device that measures angular velocity, providing information about how an object is rotating. It is a critical component in many navigation and stabilization systems, commonly used in smartphones, drones, and IMU (Inertial Measurement Unit) sensors. Gyroscopes rely on the principle of conservation of angular momentum, meaning that when an object is rotating, it will maintain its orientation unless acted upon by an external force [39] [40].

Gyroscopes typically consist of a rapidly spinning rotor mounted in such a way that it can freely move along one or more axes. As the object containing the gyroscope rotates, the gyroscope detects changes in orientation by measuring the rate of rotation around the X, Y, and Z axes. Modern gyroscopes are often implemented using MEMS (Micro-Electromechanical Systems) technology, which allows for smaller, more robust designs [41].

Gyroscopes work by detecting the rate of angular velocity (usually measured in degrees

per second or radians per second) [42] [43] about one or more axes. MEMS gyroscopes, which are widely used in modern electronics, utilize the Coriolis effect to detect rotation. Inside a MEMS gyroscope, a vibrating element is set into motion. When the system experiences angular rotation, the Coriolis force causes the vibrating element to shift [44], and this shift is detected by capacitive sensors. The degree of shift correlates to the rate of angular velocity.

In IMU systems, gyroscopes are combined with accelerometers to calculate orientation in space. While accelerometers provide information about linear motion and gravity, gyroscopes help track the rotation [43]. Together, they can be used to compute the object's Euler angles that describe its orientation as following the equations 2.9, 2.10 and 2.11.

$$\phi(t) = \phi(0) + \int_0^t \omega_x(\tau) d\tau \quad (2.9)$$

$$\theta(t) = \theta(0) + \int_0^t \omega_y(\tau) d\tau \quad (2.10)$$

$$\psi(t) = \psi(0) + \int_0^t \omega_z(\tau) d\tau \quad (2.11)$$

In practice, however, the data from gyroscopes tends to drift over time due to integration errors. To overcome this, data from the accelerometer and magnetometer (if available) is often fused with the gyroscope data using filtering algorithms such as Kalman filters or complementary filters.

2.4 Hardware

Hardware and computational power vary significantly across different microcontrollers and embedded systems, each catering to specific needs and applications. Arduino boards, like the Arduino Uno, are known for their simplicity and ease of use, making them ideal for beginners and projects with low computational needs, typically running at 16 MHz with

limited memory [45]. ESP32 offers a substantial boost in computational power with dual-core processors running at 160-240 MHz, built-in Wi-Fi, and Bluetooth, making it suitable for Internet of Things (IoT) applications [46]. Peripheral Interface Microcontroller (PIC), commonly used in industrial applications, provide a wide range of models with varying power, from simple 8-bit processors to more advanced 16-bit and 32-bit options, offering flexibility in terms of memory and performance [47]. Another architecture is the ARM microcontrollers, such as the Cortex-M series, deliver higher processing power and efficiency, often operating at several hundred MHz, with more memory, advanced peripherals, and low power consumption, making them suitable for complex real-time applications [48]. Lastly, Raspberry Pi boards, particularly the newer models like Raspberry Pi 4, feature multi-core ARM CPUs that can run at 1.5 GHz or higher, offering a full-fledged computing platform capable of running a Linux-based Operational System (OS), making them suitable for tasks requiring higher computational power, such as image processing, AI, and edge computing [49]. Each of these platforms serves a specific purpose depending on the computational demands and complexity of the project at hand.

Mind in the processing values for the controllers algorithms and features to read the value of the sensors, the main choice for hardware in the development of an platform is the hardware with basic communication protocols and a considered clock to make more operations in short time. A simple Arduino UNO can be solve the problem, on the other hand an ESP32 is more powerful and the price is not more expansive than an Arduino. Another advantage of the ESP32 over arduino boards, is the connectivity available, teh development boards of ESP32 are composed with Bluetooth Low Energy (BLE) or Wireless Fidelity (Wi-Fi) connectivity, making better to implement future applications. PIC microcontrollers are the most cheaper microcontrollers but process just with 8 or 16 bits, and the mathematical equations for this platform need to use floating point values for more precisely values for Pitch and Roll angles. Finally, Raspberry is the most powerful between then, such as a close to computer this board easily can made the processing of the platform system, however, the price does not compensate for the cost-benefit ratio, as a cheaper board already performs the necessary processing.

As discussed the better development board to implement this system is the ESP32, mind in a second possibility the Arduino also can use to this system. The priority of ESP32 to develop projects is due the possibility to expand the system for IoT platforms and integration with other projects. Also ESP32 have a great power processing with 32-bits. This allows this system to cooperate with other robots, such as precision landing missions assisted by the self-leveling platform.

2.5 Controllers

In context of robots, controllers are necessities to keep machines work precisely, and have two of controllers, in open loop or closed loop, in the Figure 2.16 shown the two topologies, in (a) the open loop were the controller do not correct the error, it means the disturbance over the system generate more errors in the output. On the other hand in (b) the topology have a feedback from the output, it means the controller correct the output according to the error [50].

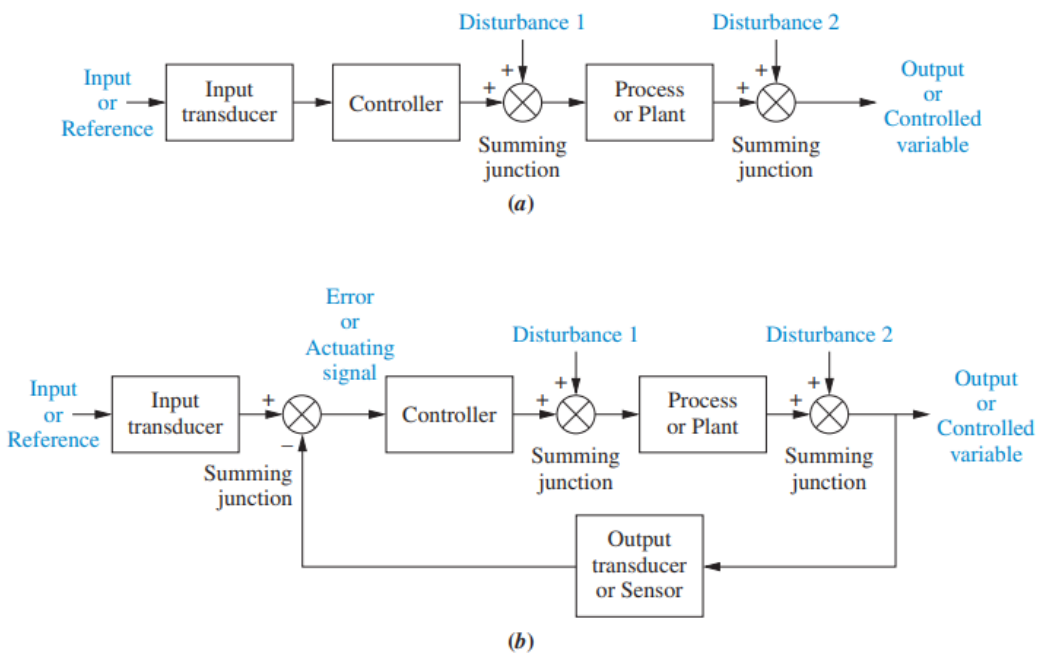


Figure 2.16: Control Diagram Topology [50]

2.5.1 PID controller

The most used controller in industries is the PID controller due to its robustness and simplicity of implementation [51]. The PID controller is a negative feedback-based control loop mechanism using the topology (b) in the Figure 2.16, this controller generate the signal for system following the mathematical equation 2.12 [52] [53], due the negative feedback the controller converge to the set point value with different behaviors according to the values of the parameters shown below.

$$u(t) = K_p e(t) + K_i \int_0^{\tau} e(t) dt + K_d \frac{de(t)}{dt} \quad (2.12)$$

were:

- $u(t)$: signal output
- K_p : Proportional gain
- K_i : Integral gain
- K_d : Derivative gain
- $e(t)$: Error signal, provided by Set Point minus feedback signal

Also it is possible to write the equation 2.12 with the standard form, were the terms K_i and K_d are write as a relation of K_p . The equation 2.13 [52].

$$u(t) = K_p \left(e(t) + \frac{1}{T_i} \int_0^{\tau} e(t) dt + T_d \frac{de(t)}{dt} \right) \quad (2.13)$$

were:

- T_d : The time in seconds to predict the error value
- T_i : The time in seconds with the intention to eliminate the error

The equation 2.13 solves for continuous time, however nowadays almost all systems are controlled with computers, and this computers can only sample data by period, so

the PID controller need fit to discrete time, were 2.13 can be write as following 2.14 [52] [54] [53].

$$\dot{u}(t_k) = K_p \dot{e}(t_k) + K_i e(t_k) + K_d \ddot{e}(t_k) \quad (2.14)$$

Developing the equation 2.14 with the approximation of the derivative with the following formula in 2.15, the final equation is following 2.16.

$$\dot{f}(t_k) = \frac{f(t_k) - f(t_{k-1})}{\Delta t} \quad (2.15)$$

$$u(t_k) = u(t_{k-1}) + \left(K_p + K_i \Delta t + \frac{K_d}{\Delta t} \right) e(t_k) + \left(-K_p - \frac{2K_d}{\Delta t} \right) e(t_{k-1}) + \frac{K_d}{\Delta t} e(t_{k-2}) \quad (2.16)$$

Each gain term change specific behaviors trough the output. The proportional gain multiply directly the error, so this term reduce the rise time, on the other hand high gain generate high overshoot, in contrast small gain generate a slow response on output. The integral term contributes to the magnitude of the error so high values of integral gain generate more oscillations, however this term acts by eliminating the steady state error. The derivative term reduces the oscillation on the output, on the other hand decrease a the settling time [53], this is the unique term that can not use solo, due this term act over the variation of the error.

This controller can be optimized changing this values, according to the parameters of rise-time, overshoot, settling time, steady-state error and stability. To tune to the optimal values, there are some optimization methods, some of them are described in the table 2.1 [52].

The main methodology to tune the controller using this table, is changing one parameter each time, starting with proportional gain, after increase or deacrease the derivative gain and finally the integral gain. Ki is the gain you need to be most careful when changing because the accumulation of error can cause instability if this gain is too high [55].

Parameter	Rise-Time	Over-shoot	Settling Time	Steady-State Error	Stability
K_p	Decrease	Increase	Small change	Decrease	Degrade
K_i	Decrease	Increase	Increase	Eliminate	Degrade
K_d	Minor Change	Decrease	Decrease	No effect in theory	Improve if K_d small

Table 2.1: PID Tuning Parameters [52]

Chapter 3

System methodology

The development of the project is based on two scenarios, how the platform intend to couple on a mobile robot, the self leveling need to correct regular and irregular grounds that the UGV can drive. Based on these scenarios, the development can separate in five parts described below:

- Physical construction of the platform prototype.
- Kinematics Analysis of the platform.
- Hardware Assembly.
- Software development.
- Test and Validation.

3.1 Physical construction of the platform prototype

About the construction of the prototype, the main point is the type of structure to mount and the kinematic behavior of the structure, dynamic behavior is also of interest when the project application is specified, in the case of this work the application is for small drone landings, having a simple dynamic as the weight load on the platform does not demand effort from the engine so that the even stabilize the platform at desired angles.

Based on that, a bidirectional platform can carry the small UAVs and have a simple kinematics behavior, also the components to mount the platform are cheaper than the other platforms due the number of actuators.

In the construction of an prototype, a Three Dimensional (3D) model is the first step to analyze the material and how to mount the prototype. With the 3D model it is clear what the materials type, shapes and how to assembly in the prototype. The Figure 3.1 shows the model of the platform prototype proposed to mount.



Figure 3.1: 3D model of platform

To mount the platform according to the model in Figure 3.1, the most parts was printed using 3D printers using PLA plastic, other parts was used Polyvinyl Chloride (PVC), wood boards and some mechanical parts that are universal and sold in market like the universal joint to fix two parts with a movement of 2 DoF

3.2 Kinematics Analysis of the platform

The model have 2 actuators on x and y axis, do they directly change the Pitch and Roll angles, generating a direct relationship between the engine position and its corresponding angle. This behavior of the bidirectional platform made the kinematics relation according to the trigonometric relations in the mount layout. So each angle is a function of each motor position

$$\phi_{Pitch} = Motor_y(\theta_y) \quad (3.1)$$

$$\phi_{Roll} = Motor_x(\theta_x) \quad (3.2)$$

The yaw angle is supposed to be 0 throughout the platform movement, but this angle depends on the robustness of the platform construction. The parts for fixing the platform with the base and engines were produced with PLA plastic, which can suffer slight twists without the parts breaking, thus the Yaw angle is close to 0, suffering only from system disturbances.

3.3 Hardware Assembly

To control the entire system, a micro-controller and drivers for the motors are needed, in addition to sensors for closed-loop control. The specification of the system's electronic components depends on the project specifications, due to the need for position control, stepper motors were chosen as actuators for movement control. To measure the Pitch and Roll angles, the IMU is enough once the Yaw angle is not necessary to measure, to read the values from the sensor the micro-electromechanical systems (MEMS) devices has communication protocols such as Inter-Integrated Circuit (I2C) or Serial Peripheral Interface (SPI), this is a important feature to consider for choose the micro-controller. Other considerations for the hardware system are the motor drivers that support the power consumption of the servo motors, and the power supply conversion.

Based on all those components necessaries to assembly the hardware system, the following components in the table 3.1 are chooses

Component	Part Number
Motor	Nema17 with planetary gear box
Motor Driver	DRV8825
Micro-controller	ESP32
Sensor	ADXL345
Supply	12V Battery
Supply converter	LM2596 Buck Converter

Table 3.1: Hardware Components List

3.4 Software development

The Software is developed based on the hardware components in section 3.3, in Figure 3.2 shows how information travels from the sensor to the motor drive to control the angle of interest.

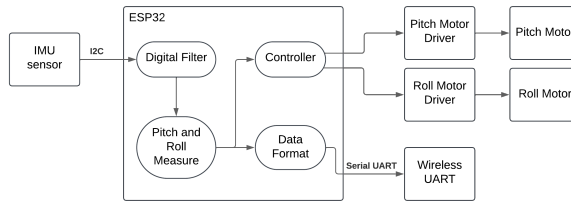


Figure 3.2: Block Diagram of the system

In this diagram it is possible to see 3 paths that the micro-controller need to manage, 2 of these paths are the signal for the motor drivers, and those signals came from the same function, which is that of the controller function, so these tow signals can be managed with a unique flow code. The other path is the data transmit to collect the information of the slopes. Collect data is important to plot the behavior of the platform and make another analysis.

To manage this flow, a timer is necessary to call the functions in a fixed period, how the dynamic of the motors are slow due the gear box reduction, a small frequency like 100 Hertz (Hz) for call the functions is enough. So each 10 ms the sequence of funtions called are the following order:

1. Sensor Measure and filtering

2. PID Function

3. Data Transmit

But one more timer is necessary for this system, which is responsible for generate the signal for the step motor drivers, how the driver can response a minimum period of 4 microseconds (μs) according to the datasheet [56], how the PID function is called with a fixed period, the timer that is responsible to control the motor drivers can be generate the signals for both drivers in this time, but with different number of steps and different speeds, once the pulse width for one step can be $4 \mu s$. So the maximum number of steps that can be runned by the motor between the PID cycles is 2500 steps, with the planetary gearbox reduction the maximum speed is 452,46 Rotation Per Minute (RPM), the datasheet [57] informs that the engine can reach speeds of up to 3000 RPM. However, the physical motor cannot response this speed.

The IMU sensor measures acceleration in all 3 axes, and this raw data is read with noise. To avoid this noise, an exponential moving average filter was used due to the low computational processing required and a good response to filter out high frequencies.

3.5 Test and Validation

To validate the platform functionality and kinematics, those two ways can validate the position of the platform, where the second is considered the true ground, due the position of the motor have a relation with the slope angle.

- Reading the sensor on the platform
- Calculating the roll and pitch angle with kinematics relation

The reliability of the sensor's reading depends on its calibration and the quality of its data filtering. to calibrate the sensor, the true ground is the kinematic mathematical relation of the slope and the motor position, and the way to measure the motor position

can be used a simple protractor to validated the sensor measures. Once calibrated taking into account the offset error, the sensor's readings are reliable for use in tests.

Chapter 4

Development

The development was organized into prototyping of the physical structure, hardware implementation and software development.

4.1 Physical Structure

The first step was mount the physical platform, after desing all parts in 3D, some parts are printed in 3D Printer using PLA filament, and the other parts are bought in market. The parts printed are:

- Lower Brackets
- Upper Brackets
- Central Support
- Joint Coupler
- Motors Supports
- Battery holder

Each part are shown in the Figure below, as 4.1a, 4.1b, 4.1c, 4.1d, 4.1e and 4.1f respectively to the previous list

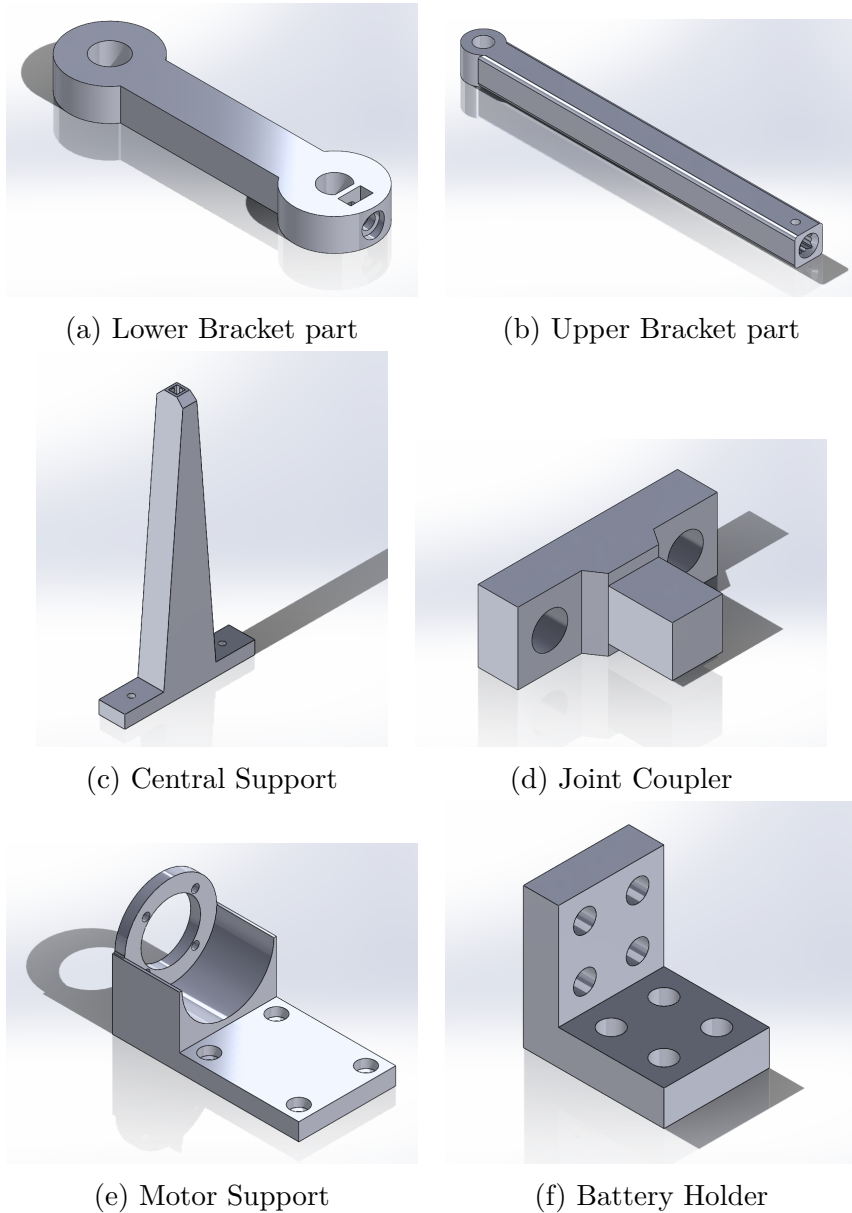


Figure 4.1: Mechanical parts printed using PLA filament

The other parts consist of a wooden base for attaching the platform, a PVC plastic sheet for use as a landing pad or for other purposes, screws, NEMA17 motors and universal joints.

The universal joints allow movement in two directions, this is necessary for each axis due to the two degrees of freedom the platform has. Since it needs 3 points to support the plane of the platform, 3 universal joints are used, on both brackets and on the central support, the Figure 4.2 below shows the joint used in the prototype.



Figure 4.2: Universal Joint

The prototype of this platform was assembled as shown in the image 4.3 below.

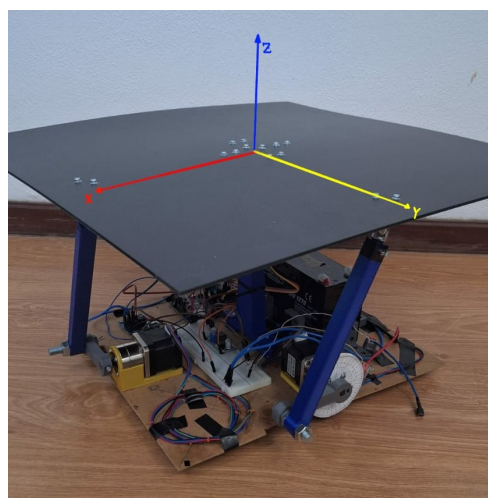


Figure 4.3: Physical platform with reference

The structure was assembled according to the layout shown in images 4.4 and 4.5, using the following distance and length values shown in the table 4.1. These lengths were guaranteed due to the precision of 3D printing, where printer error is very low guaranteed by manufacturers.

Feature	Value (mm)
h_{cs}	187.35
L_1	70
L_2	200
d	200

Table 4.1: Lengths of structure parts

With these values, the kinematic behavior of the platform can be analyzed with the equations below. For the kinematic analysis, it is first necessary to analyze the layout of the structure with the measurements and variables involved, as shown in the Figures 4.4 and 4.5 below.

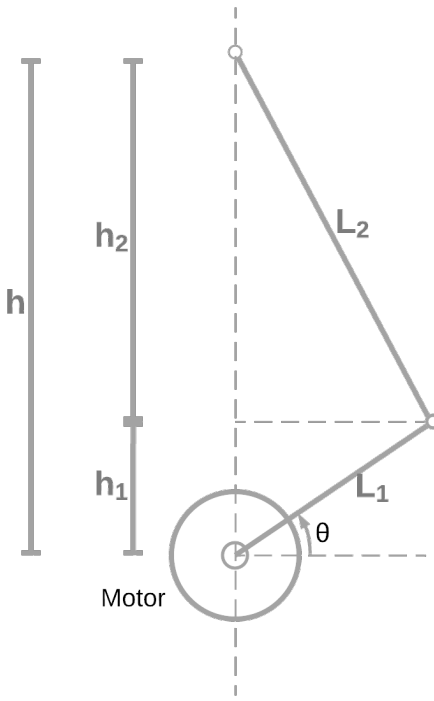


Figure 4.4: Frontal view of the platform [25]

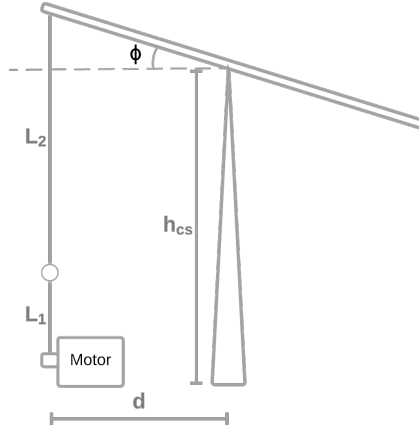


Figure 4.5: Lateral view of the platform

In Figure 4.4, is possible to take the relation of the total height of the platform is following 4.1

$$h = \sqrt{L_2^2 - L_1^2} \quad (4.1)$$

Looking with another perspective for the platform, that the Figure 4.5 shown, the slope of the platform is related by the following equation 4.2.

$$\phi(\theta) = \arctan \frac{h(\theta) - h_{cs}}{d} \quad (4.2)$$

Where $h(\theta)$ is given by (4.3)

$$h(\theta) = L_1 * \sin(\theta) + \sqrt{L_2^2 - (L_1 * \cos(\theta))^2} \quad (4.3)$$

This equation is valid for both angles, and makes it easier to validate the inclination of the platform since there is a relationship between the position of the motor and the inclination, where:

- θ is the position of motor
- ϕ is the slope angle (Pitch or Roll)

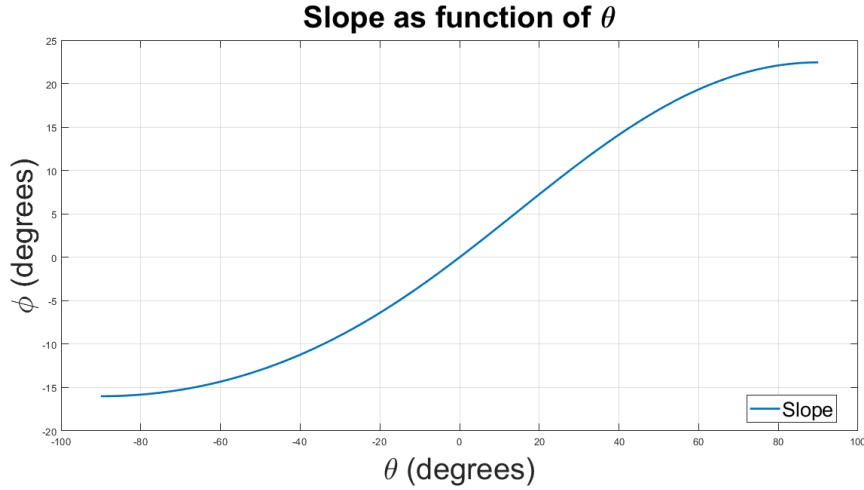


Figure 4.6: Slope function

in the graphic is possible to see a maximum of 22.5 degrees and minimum of -16 degrees of slope. Using this graphic as a true ground, it is possible to validate the measures from the sensor.

4.2 Hardware Implementation

The guide of all hardware assembly is the circuit schematic, made with the software KiCAD the following schematic in Figure 4.7 shown the connections of the main system.

The use of modules makes it easier to connect the components, and the module for the stepper motors is a key item for assembling the hardware. A board was used which, as well as having DUPONT connectors, comes with Dual In-line Package (DIP) switches for selecting the microsteps. The other connections between the modules and the main development board, the ESP32, were made using normal jumpers. To control the two motores, the DRV8825 step driver module was used one for each motor, this module need 2 pins from the microcontroller, the step pin and the direction pin. The step pin is active in rising edge, while the direction pin control the direction of the motor based on the logic level of the pin, where at low level it rotates in one direction while at high level it rotates in the opposite direction.

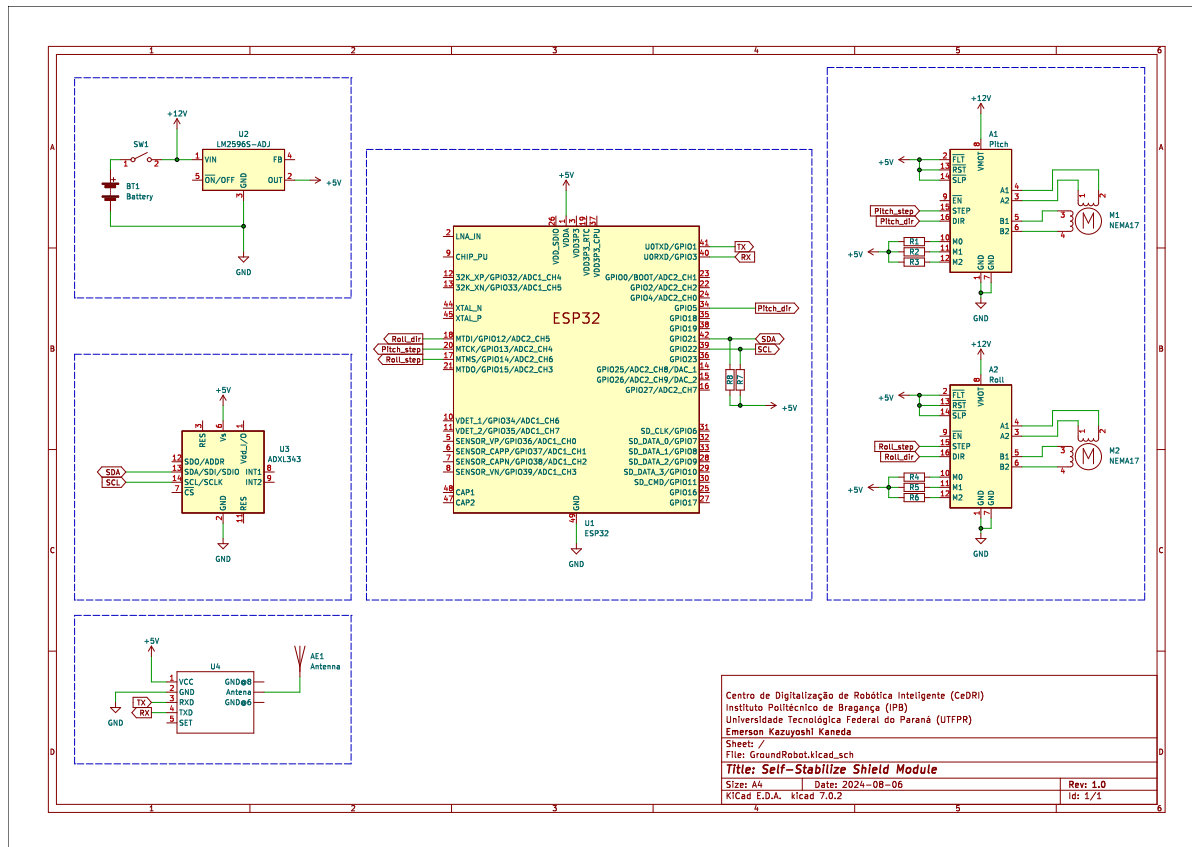


Figure 4.7: Circuit Schematic

Ideally, it would be best to develop a Printed Circuit Board (PCB) as a shield for the ESP32, but for this it would be interesting to analyze other possible devices and modules that could be implemented as additive functions in the system, so that the cost of producing a PCB is cost-effective.

As the platform uses motors, it is necessary to pay attention to the electric current coming from the power sources of the motors, as they produce current peaks due to their inductance and can produce a reverse current due to the counter electromotive force. To solve this problem, protection is used between the battery and the drivers, which can be a simple diode for each module.

To read the sensor, the I2C protocol was used, which consists of using two microcontroller pins to communicate with up to 127 devices addressed on the bus, the Serial Data (SDA) and Serial Clock (SCL) pins. In this case the device is an ADXL345 3 axis accelerometer, the address of this sensor is 0x53 by default, it can be changed setting the pin ALT ADDR to high, and the new address is 0x1D.

The last module used in the platform is the wireless Universal Asynchronous Receiver/Transmitter (UART) protocol communication, this module is optional for the functionality of the platform, on the other hand this module made easier the data collection to analyse the behavior of the slope. Using the Hayes commands, also known as AT commands, it is possible to configure the baud rate of the module, by default 9600 bits per second (bps) is used, but the lower the baud rate the greater the communication distance between the modules. As the focus is on use outdoors and coupled to a mobile robot, the best to use is the lower baud rate of 1200 or 2400 bps to grant a farthest communication.

4.3 Software Implementation

For better visualization during software development, an important tool is the use of flowcharts. In this work, the software was based on 2 flowcharts, one being the data flow and the other the motor control diagram. Figure 4.8 below shows the data flow from sensor reading to motor actuation, and Figure 4.9 shows the implemented control

diagram.

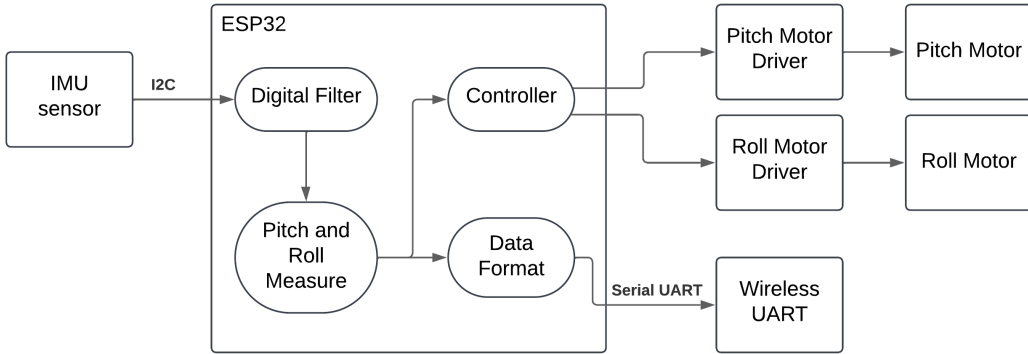


Figure 4.8: Flowchart of data travel

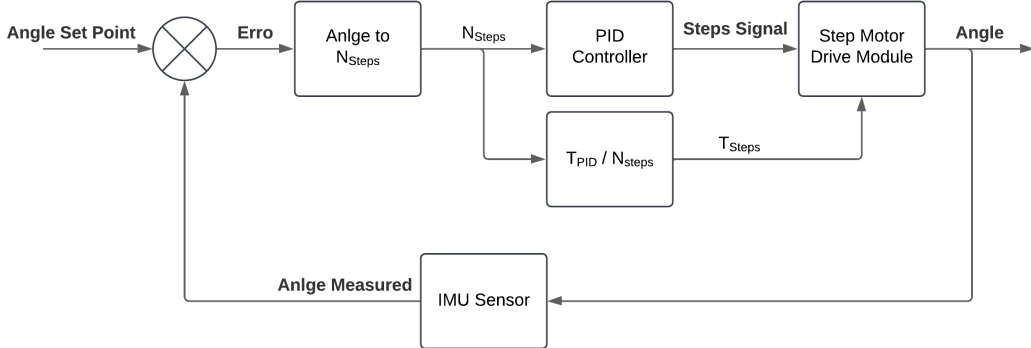


Figure 4.9: Control Diagram

To develop the software, the ESP32 was programmed using the PlatformIO tool, which is an extension of VSCode for programming various microcontrollers. This extension allows you to choose which development board will be programmed and which framework will be used to program the device. In this work, the Arduino framework was used.

4.3.1 Measuring Data and Calculating Angles

Starting with the IMU sensor, the ADXL345 already has a library for reading the acceleration values in the 3 axes. The library used was Adafruit_ADXL345_Unified [58], the data sample rate is the same period of the PID control function, but the samples need to

collect the data and filter the data before the control function call. This period is 10 ms so the sample rate is 100 Hz as cited before.

The IMU sensor measure the accelerations of the 3 axis (x, y and z axis), and this raw values have a high, how the main signal is a low frequency the use of an move average filter is valid due the low computer consumption and fast response with low number of samples. To optimize the filter a exponential move average is a good option, because the buffer for the past values is not necessary anymore in this filter, just the last value filtered, so the time to calculate the filter do not need a loop to calculate. The equation 4.4 shows the mathematical response of the filter.

$$y[0] = \frac{y[-1] * N + x[0]}{N + 1} \quad (4.4)$$

Were:

- $y[0]$ is the new value filtered
- $y[-1]$ is the last value filtered
- $x[0]$ is the new value measured from sensor
- N is the deep of the filter

This equation was implemented using the filter depth N with the value 15, it was tested with the values 1, 3, 7, 15 and 31, and the best answer that reduced vibration noise while maintaining a low delay at the filter's output was the value 15.

After filtering out the high frequencies in the acceleration signals, the next step according to the information flow in 4.8 is to calculate the Pitch and Roll angles, using equations 4.5 and 4.6 below to calculate the respective angles.

$$Pitch = \arctan\left(\frac{a_y}{\sqrt{a_x^2 + a_z^2}}\right) \quad (4.5)$$

$$Roll = \arctan\left(\frac{-a_x}{a_z}\right) \quad (4.6)$$

With the two angles calculated, it is possible to proceed with the PID calculation.

4.3.2 PID Development

According to Figure 4.9, the first step is to measure the error, which is just a subtraction between the set point and the previously calculated angle value, after which it is necessary to convert the angle to the number of steps so that the controller can send a number of steps to the motor drivers. This conversion is a simple calculation of the calculated error divided by the angle generated per step, the stepper motor used is a NEMA 17 in which each step the axis moves 1.8 degrees, however with the driver configured for 32 micro steps and the reduction gearbox, each step moves $1.8 / 32 / 5.18$ resulting in approximately 0.01 degrees. Then the conversion from angle to number of steps is done using the equation 4.7 below.

$$N_{step} = \frac{\phi_{err}}{\theta_{step}} \quad (4.7)$$

Where ϕ_{err} is the error calculated before and θ_{step} is the angle per step calculated previously, its value being 0.01 in the present work.

With the number of steps calculated we have 2 controllers implemented, one being a position control, in which it performs the PID calculations of equation 2.12, and the other control being a proportional speed controller changing the period of the steps with each iteration of the controller, the speed controller is to have a smoother step response which will be discussed in the results section.

The speed controller was developed based on the period of the PID cycle, due to the following reasoning, every time the controller performs its calculations it generates an increment or decrement in the number of steps that the motors need to perform, so that the number of steps does not accumulate with the amount previously calculated, the calculated steps need to be performed before the next iteration of the PID, thus the controller has its output according to equation 4.8 below.

$$T_{step} = \frac{T_{controller}}{N_{step}} \quad (4.8)$$

After the controller has performed the position and velocity calculations for both motors (X and Y), the microcontroller needs to send the signals to the motor drivers. To do this, we used a timer with a period of $2 \mu\text{s}$ to change the state of the microcontroller pin (so the period of signal is $4 \mu\text{s}$), which corresponds to the minimum response period of the DRV8825 controllers, according to their datasheet. Although the period of the signals varies due to the speed controller, it was implemented at the maximum frequency that the driver can support, since this speed is limited by hardware limitations so its the maximum speed the motor can reach.

4.3.3 Data Transmit

Finally, the communication system for data collection used the ESP32's own serial communication. Thinking about coupling the platform to mobile robots, so that there is the possibility of data collection without the use of cables, the HC-12 module was used, which is a wireless communication module using the UART protocol. This module can configure the Baud rate and channel using the Comandos Hayes Commands (AT commands), so before assembly in the hardware is necessarie configure the module, and was cofigured to use channel 1 and 2400 bps to reach far distances.

The arduino framework send datas to serial comuniction with the method `Serial.print`, however this method transform the data in ASCII code, then send the package of bits, this take a lot of machine cycles, and how the angles are storaged in floating point variables, the microcontroller need to transform a huge number of characteres. To reduce the number of machine cycles and make the system faster in sending data over the UART, the following steps are done:

1. Multiply the angle by 1000 to get 3 decimal places
2. Transform the data format to `int16_t` using cast

3. Send the high and low package binarie using Serial.write()

When data is received by another system, it is necessary to treat the data by dividing by 1000 and adjusting the received packets, as the 8 Most Significant Bit (MSB) are sent first and then the 8 Least Significant Bit (LSB).

To communicate with the platform, was implemented 2 commands to cooperate with the system, one for changing the PID controller gains and the other for changing the pitch and roll angle set point.

To change the set point of the angles, the other system need to send a string to the platform over the UART serial communication, using the following format:

$$SP; \%f; \%f \backslash n \quad (4.9)$$

Were the first floating value is the pitch set point and the second value is the roll set point, is important to use a dot to separate the decimal places instead a comma, because it is how the system understand the decimal places.

To change the PID gains, is the same way, but using the following format of string:

$$PID; \%f; \%f; \%f \backslash n \quad (4.10)$$

Were the first value is the propotional gain, de second is the integral and the third value is the derivative gain.

Chapter 5

Results

This chapter will discuss the tests carried out in this work, which are listed below.

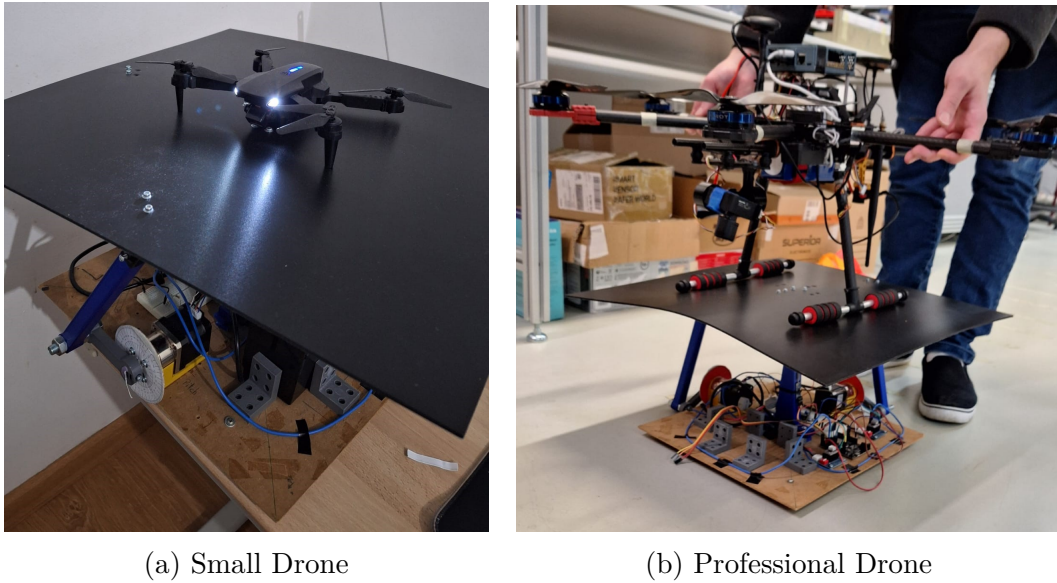
- Kinematic Validation measuring the angles
- Controller Validation
- Dynamic test using weights
- Environment test intend to couple in a mobile robot

5.1 Kinematic Validation measuring the angles

After mounting the structure according to Figure 3.1, as was shown in Figure 4.3, was checked if the platform has the area for some small drone to land over the platform, and the area of 500x500 mm was enough, as shows the Figure 5.1.

The first test is to calibrate the sensor by measuring the angles with the sensor and equipment designed for this purpose. In this case, the following level meter in 5.2 was used as the true ground.

With this level meter, the angle measured by the sensor and the actual angle measured by the level meter at a given motor position were observed, in order to analyze the offset error of the sensor and the error in relation to the structure, the following Figure 5.3 shows



(a) Small Drone

(b) Professional Drone

Figure 5.1: Drone over the platform



Figure 5.2: Angled Level Meter

how the measure was made using the level meter, first, the desired angle was set on the level gear, then the arm was adjusted until the level indicated that it was at the desired angle, and both the sensor was observed by the serial monitor and the motor position with the aid of a pointer on the arm.

The following Figures 5.4 and 5.5 show the result of the calibration of both angles, pitch and roll, to check the accuracy of the sensor and the validation of the calculated



Figure 5.3: How measured the angles

kinematics. For calibration, a level meter was used, as shown in Figure 5.3 .



Figure 5.4: Pitch Angle Calibration

Were the blue line is the level meter taking as true ground, the orange line is the angle measured by the sensor, and the green line is the angles calculated by the kinematics in 4.2.

With those two graphics, it is possible to see that the sensor has a low offset error on pitch angle, and a considered offset angle on roll. Also, is visible in the two angles both do



Figure 5.5: Roll Angle Calibration

not follow the calculated kinematics, this due the imperfection of the mechanical assembly. Another important detail in both graphs is that the two kinematics are reversed, because the pitch angle motor has been positioned on the opposite side of the platform, so the kinematics refer to $-\phi$ instead of ϕ . The kinematics of the angles measured in Figure 5.5 is validated using the previous equation 4.2 using the following values measured with a ruler tape:

- $H_{cs} = 210\text{mm}$
- $L_1 = 70\text{mm}$
- $L_2 = 240\text{mm}$
- $d = 215\text{mm}$

Using these values, the kinematics graph is in accordance with the measured angles, this can be verified in the 5.6 and 5.7 graphs.

A final consideration in this calibration stage is the measurement of the values, as an analog level meter was used, there is also a percentage of human error.

Regarding the data values obtained in the previous graphs, the maximum angle measured by the level meter and the sensor in both angles are shown in table 5.1. This table shows the range in which the motors can position the platform.



Figure 5.6: Correct Pitch Kinematic

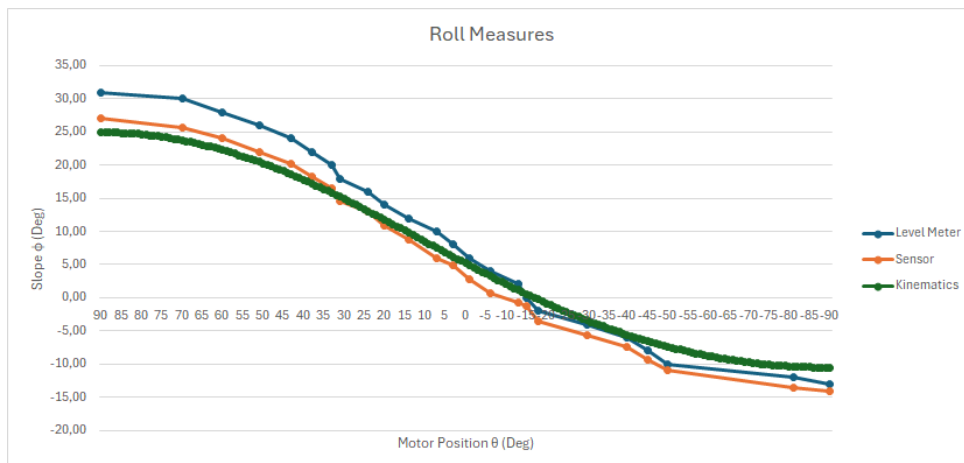


Figure 5.7: Correct Roll Kinematic

	Pitch Level Meter	Pitch Sensor	Roll Level Meter	Roll Sensor
Maximum	11°	10.54°	31°	27.07°
Minimum	-29°	-28.12°	-13°	-14.04°

Table 5.1: Maximum and Minimum angles

The difference between the maximum and minimum values indicates that the platform has a total range of 40° for the pitch angle and 44° for the roll angle, but the sensor can only measure a range of 38.66° for the pitch angle and 41.11° for the roll angle.

In relation to sensor accuracy and validation of kinematics, the mean error, Mean Absolute Error (MAE) and the Root Mean Squared Error (RMSE) between the level meter and the sensor, and between kinematics and level meter, in the previous Figure 5.4 and 5.5 are shown in the table 5.2.

	Pitch Sensor Error	Pitch Kinematic Error	Roll Sensor Error	Roll Kinematic Error
Mean Error	0.58	7.03	2.79	-6.44
MAE	0.89	7.03	2.79	6.44
RMSE	1.08	7.71	2.99	6.71

Table 5.2: Errors

This table shown the pitch sensor have a high acurracy, and this mean the pitch angle doesn't need a high value to compensate the offset, the roll sensor have a considered offset error this probally due how the sensor was fixed in the structure because the sensor module have only 2 fixing points with screws, allowing a small rotation along the axis referring to the roll measurement, however this error can be compensated in the software. On the other hand, the error between the true angle and the spected angle calculated by the kinematics have a huge error, this mean the mechanical structure need to be developed by specialist in the area.

5.2 Controller Validation

In this section, was made tests to verify the bests values for the position PID controller, the sequence of tests made are increasing the Kp first, then the Kd and finally the Ki.

5.2.1 P gain

The following Figures 5.8, 5.9, 5.10, 5.11 and 5.12 represent the system's step response with K_p equal to 0.1 and increasing by 0.1 in each test until K_p equals 0.5

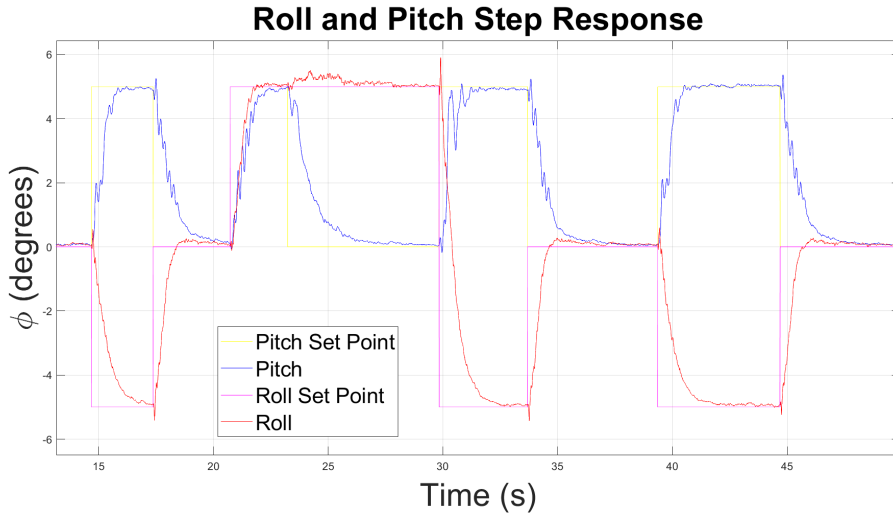


Figure 5.8: K_p equals 0.1

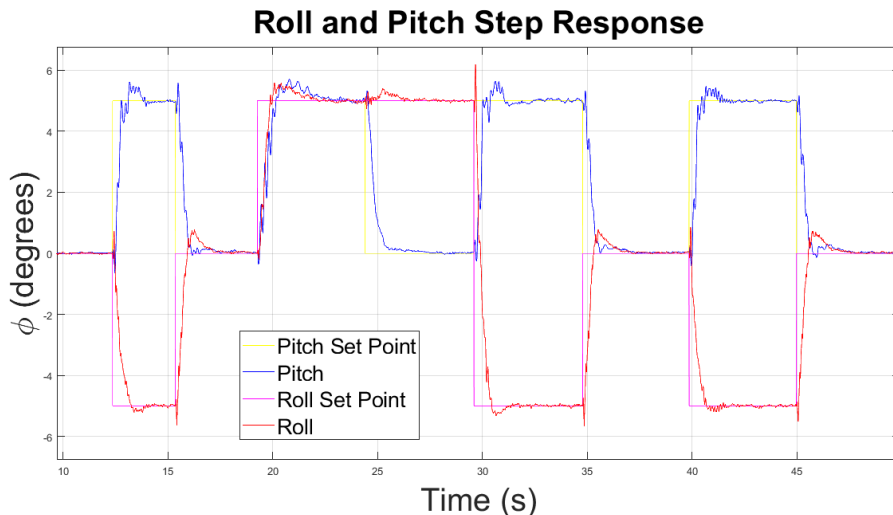
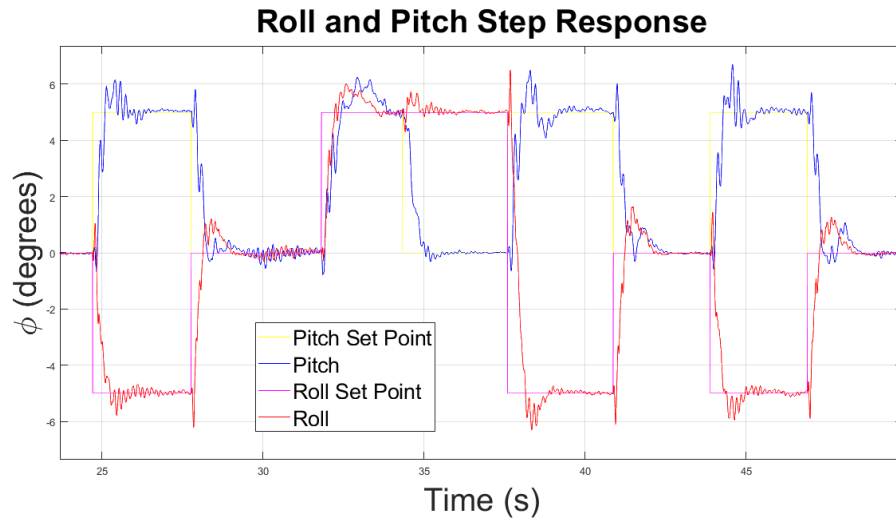
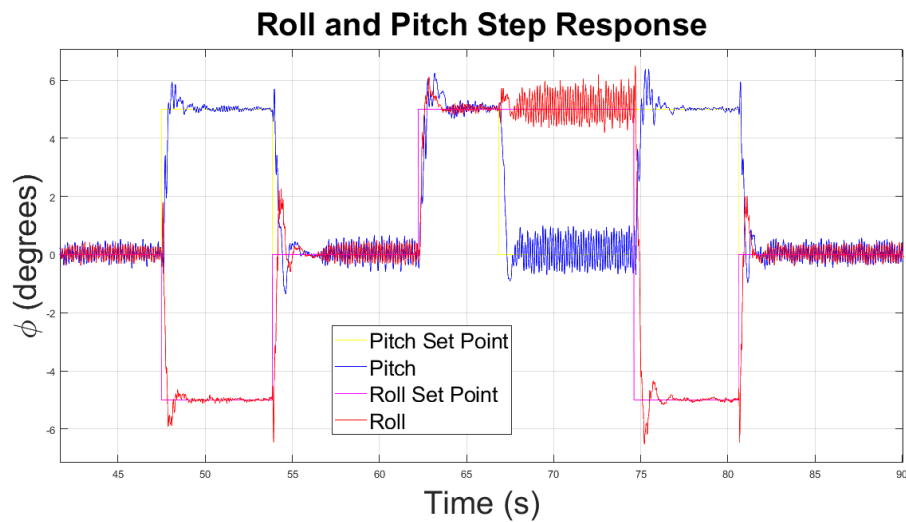
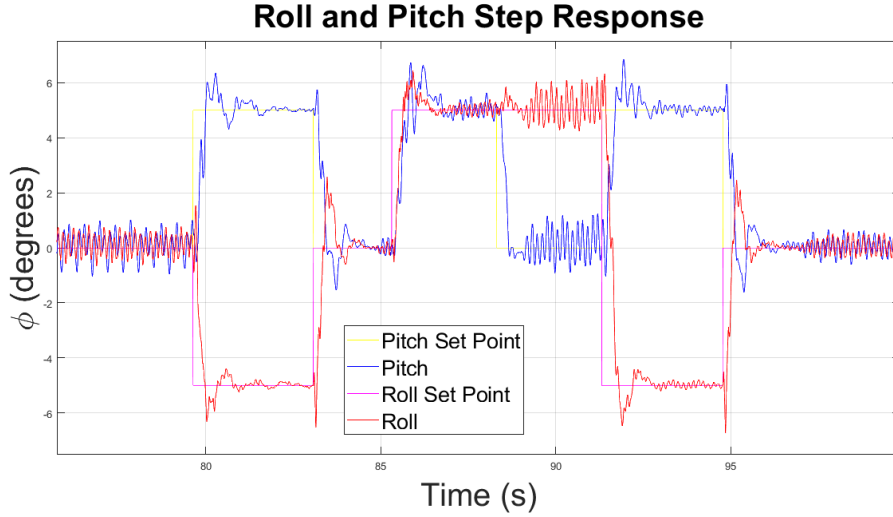


Figure 5.9: K_p equals 0.2

With lower gain, a response with low overshoot is visible as expected, while with higher proportional gain, a higher overshoot, specifically in the roll angle, is visible but with a shorter rise time. Another behavior when increasing the proportional gain was

Figure 5.10: K_p equals 0.3Figure 5.11: K_p equals 0.4

Figure 5.12: K_P equals 0.5

observed was the instability in steady state, were a high oscillation was in the response, this oscillation reach closer to 2 degrees of amplitude.

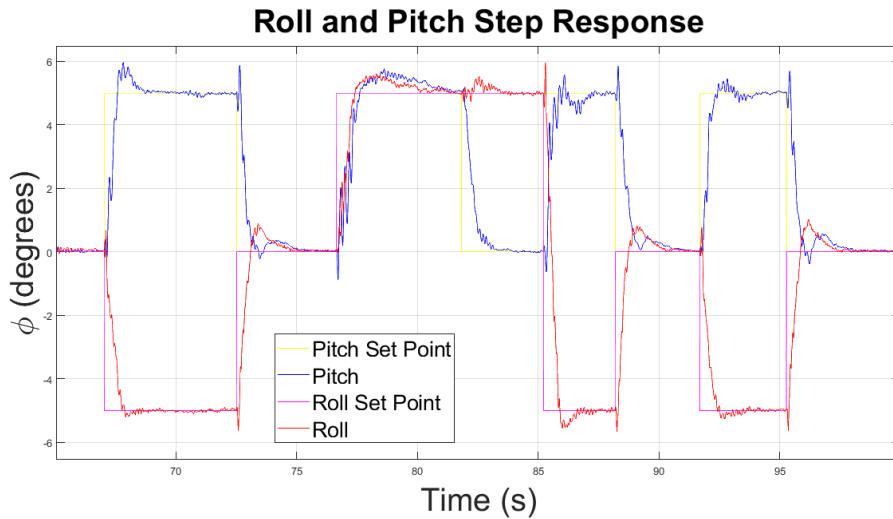
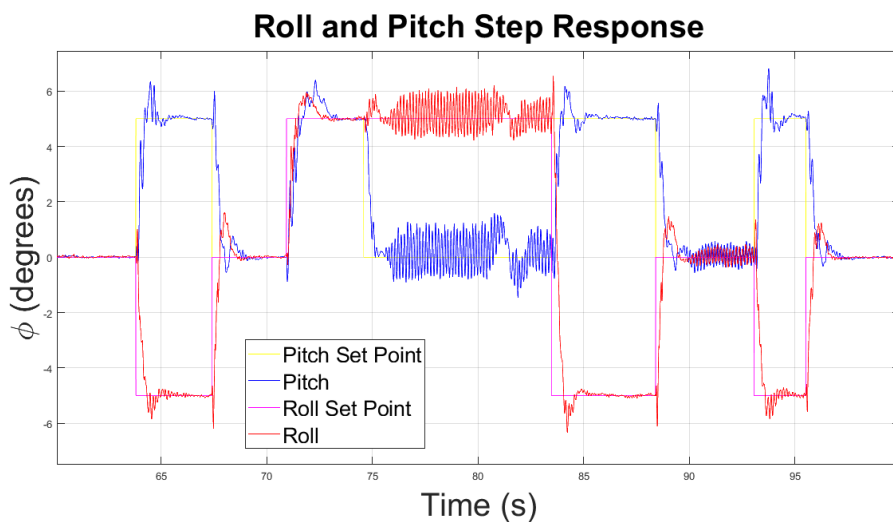
5.2.2 D gain

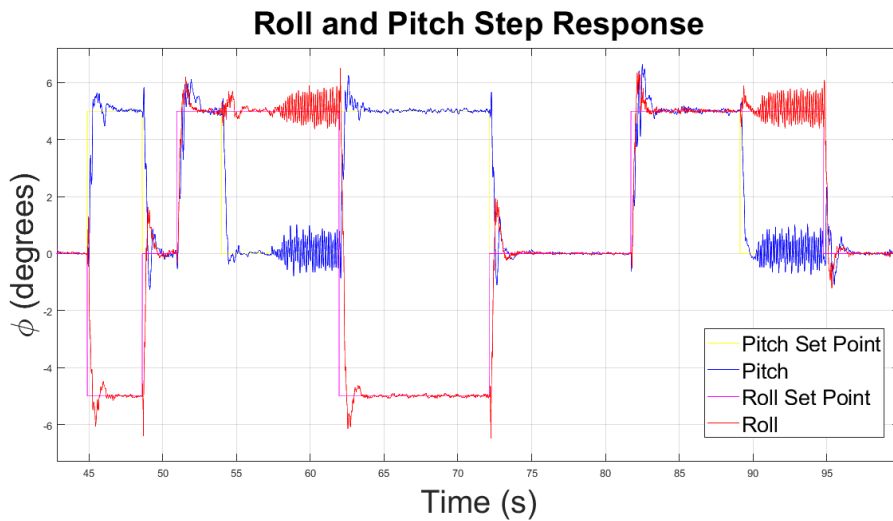
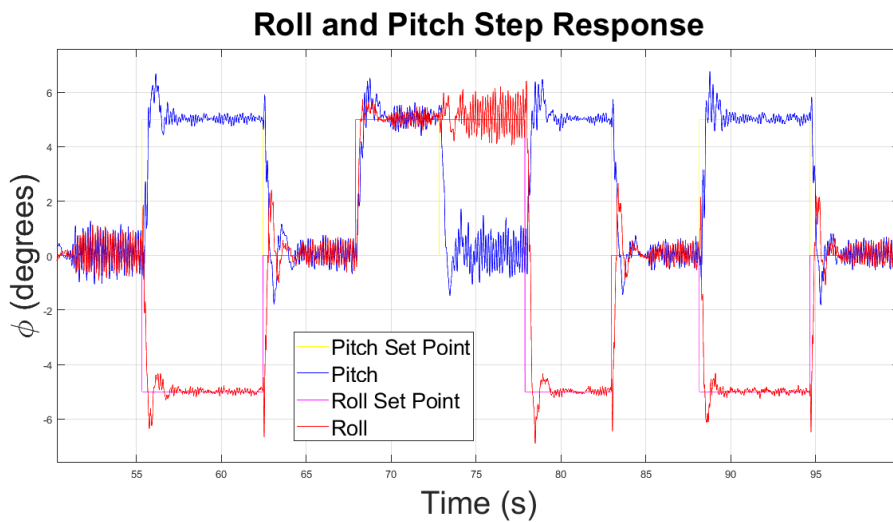
After fixing the proportional gain with the value 0.1, now it is necessary to increase the value of the derivative gain, starting with a value of 0.1 and increasing by 0.1 with each test up to 0.4 of K_D, we have the following graphs below in 5.13, 5.14, 5.15 and 5.16.

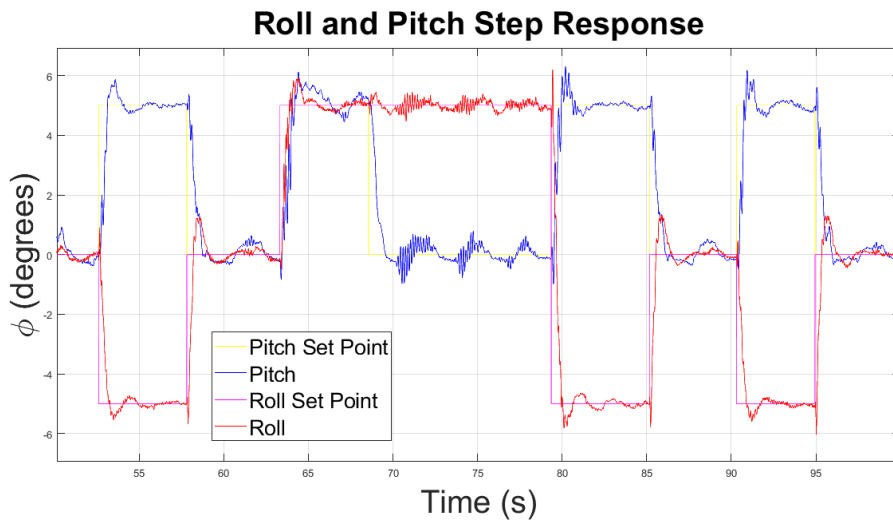
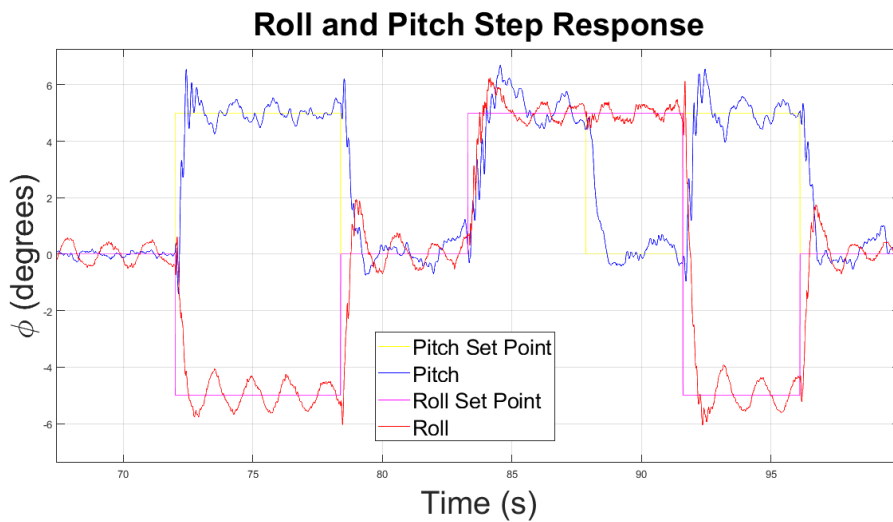
This gain has a greater impact on the transient regimes, as can be seen in the previous Figures the rise time decreased as the gain increased. When this gain has its value corrected due to calibration, there is a reduction in oscillations as seen in the Figures with the low gain, all the while as the value of K_D increases there is a noticeable increase in instability with numerous oscillations in the permanent regime.

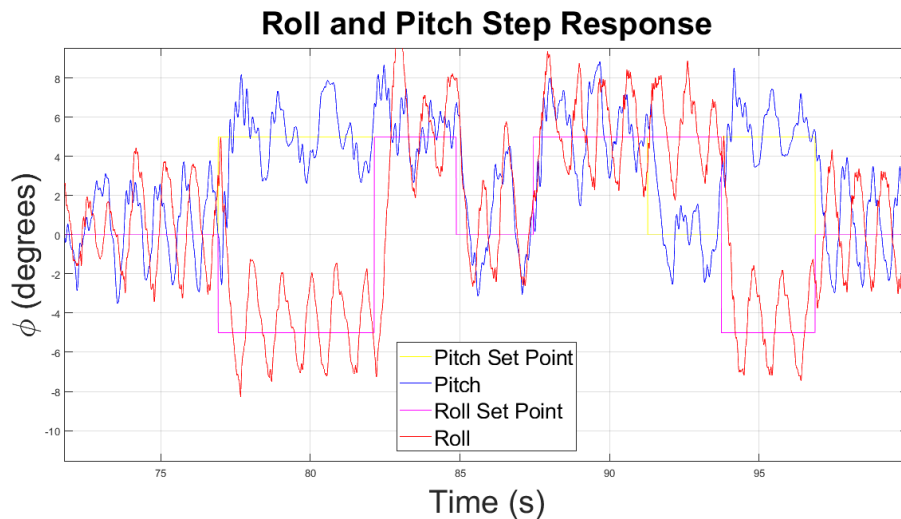
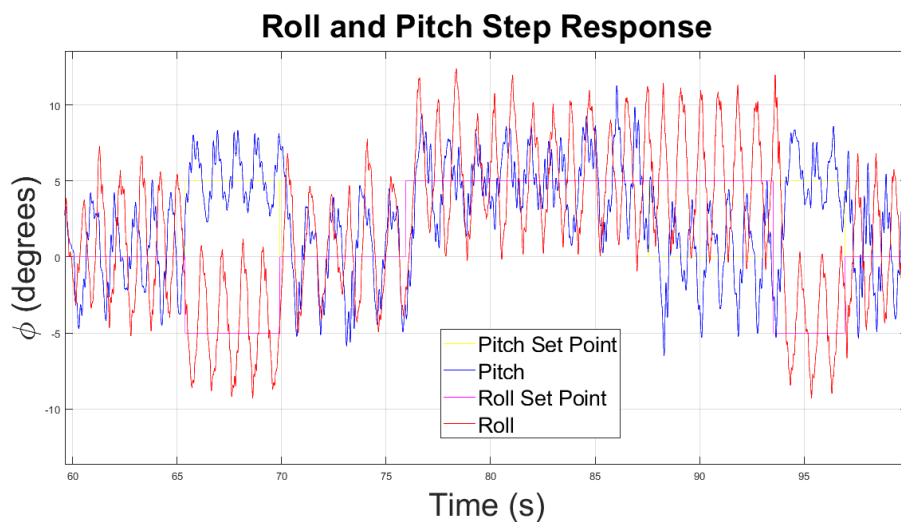
5.2.3 I gain

Finally, to increase the integral gain, was fixed the proportional with 0.8 and derivative with 0.1, then starting the K_I with 0.1 and increasing 0.2 each test, the following tests are taken in Figures 5.17, 5.18, 5.19 and 5.20.

Figure 5.13: K_d equals 0.1Figure 5.14: K_d equals 0.2

Figure 5.15: K_d equals 0.3Figure 5.16: K_d equals 0.4

Figure 5.17: K_i equals 0.005Figure 5.18: K_i equals 0.01

Figure 5.19: K_i equals 0.05Figure 5.20: K_i equals 0.1

In the first test there is already a noticeable oscillation in the response, which increases as the gain K_i increases. This is not desirable for the platform, then the integrator term of the PID needs to have a very low or zero gain, with no relevant impact on the step response.

5.3 Dynamic test using weights

The next test carried out to evaluate the platform is in relation to its load capacity. The responses to the step were tested with weights from 1kg up to 5kg with a 1kg increment in each test, with the same controller gain, in this case using the P controller with a gain value of 0.8.

The weights were placed inside a bag and this was positioned so that it was centered on the platform, so as not to require too much effort from both motors.

The Figures 5.21, 5.22, 5.23 and 5.24 shown the step response of each weight using the proportional controller gain with 0.1, unfortunately the test using 5 kg do not work, at the beginning of the test, the platform began to twist on its own axis as the motors operated, so this test was interrupted and the platform's weight limit was considered to be 4 kg.

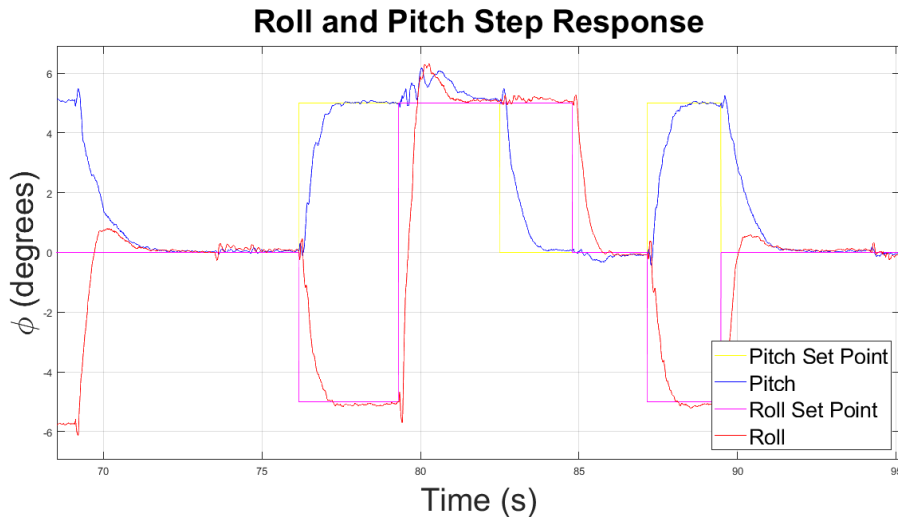


Figure 5.21: Step response with 1kg load

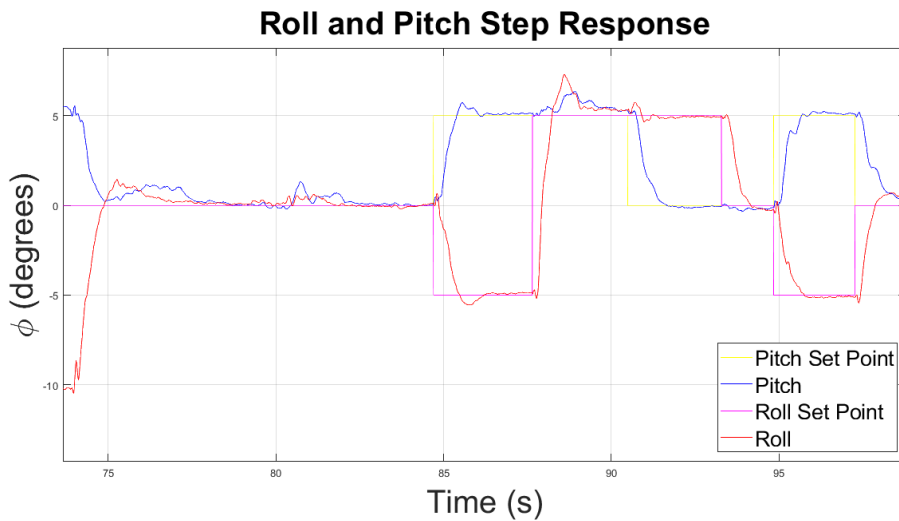


Figure 5.22: Step response with 2kg load

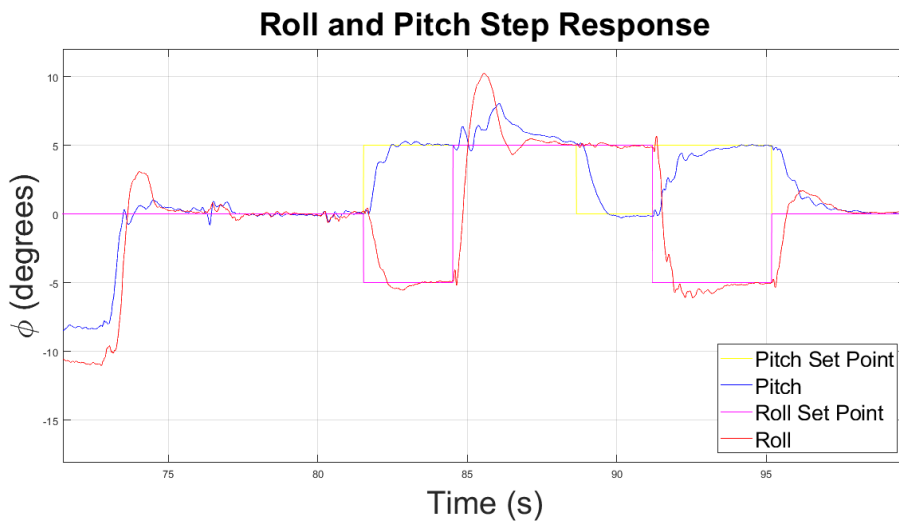


Figure 5.23: Step response with 3kg load

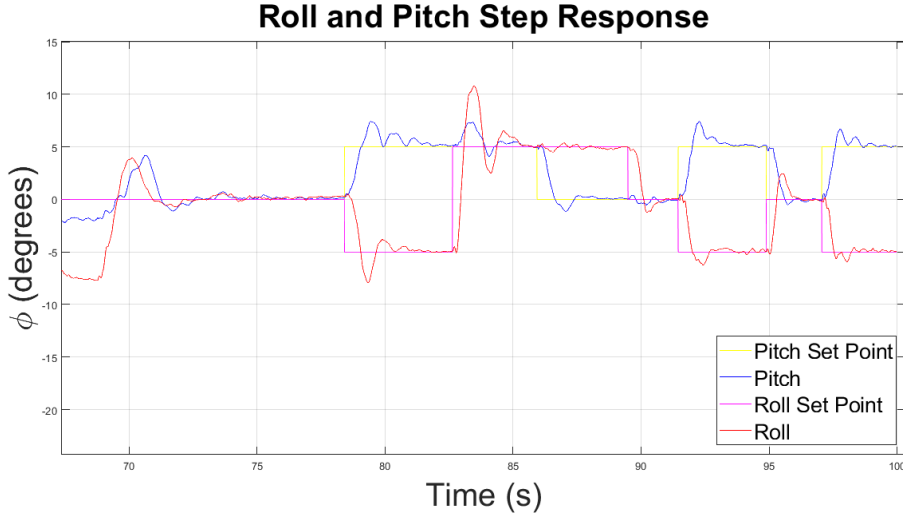


Figure 5.24: Step response with 4kg load

In the first two tests in 5.21 and 5.22, there is not much difference in relation to the no-load tests with the P controller with gain 0.1. There is only a small oscillation at steady state and overshoots less than 10%.

Unlike tests with more weight in 5.23 and 5.24, where overshoot peaks of up to 50% of the step value are noticeable.

5.4 Environment test intend to couple in a mobile robot

This section shows the test results obtained with the platform on a vehicle, simulating a mobile robot. Two types of tests related to the terrain were carried out, one in an indoor environment where the terrain has no relevant irregularities, and the other test in an outdoor environment with very uneven ground. Another test was carried out with the vehicle stationary but with the platform connected, and a drone controlled by an operator for a take-off and landing operation on the platform.

The Figures 5.25a and 5.25b show how the tests were done with the platform over the vehicle, in indoor and outdoor scenarios.

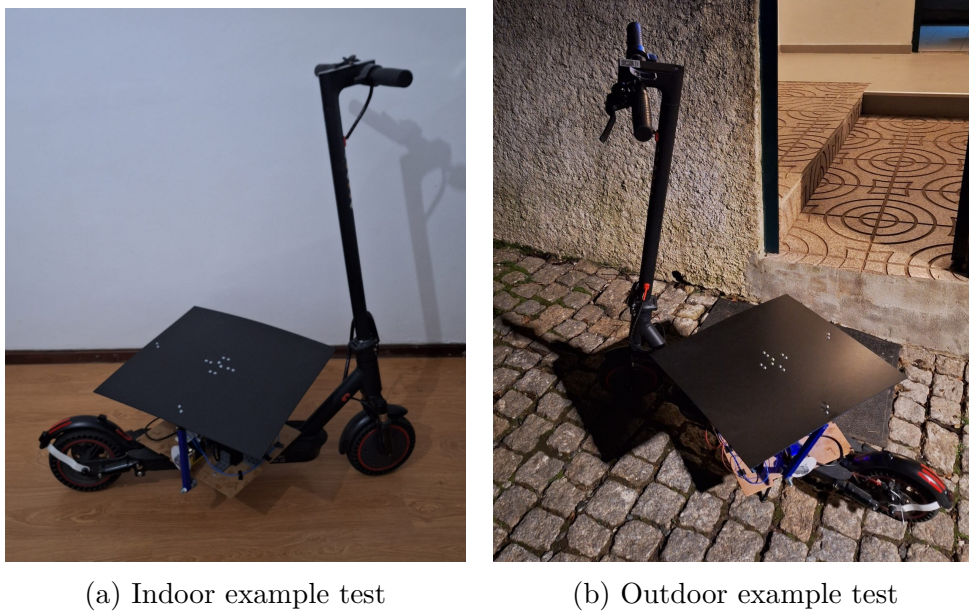


Figure 5.25: Example of Indoor and Outdoor tests

5.4.1 Indoor Tests

This test was carried out in an indoor environment with a uniform wooden floor, with good regularity or low irregularity considered negligible. Figure 5.26 shows the graph obtained from the stabilization of the platform on the moving vehicle.

The graph shows the platform trying to keep level at the set point as the vehicle moves, there are peaks of up to 6 degrees of inclination, the Mean Error (ME) and RMSE of this test are in the table 5.3 below.

	Pitch	Roll
ME	-0.3663	-0.3656
RMSE	1.7268	1.7417

Table 5.3: Indoor Test Errors

The ME and the RMSE are close to the setpoint, which means that the platform is able to level off at the desired setpoint, however the critical angles are the peaks that can cause slippage depending on the load on the platform.

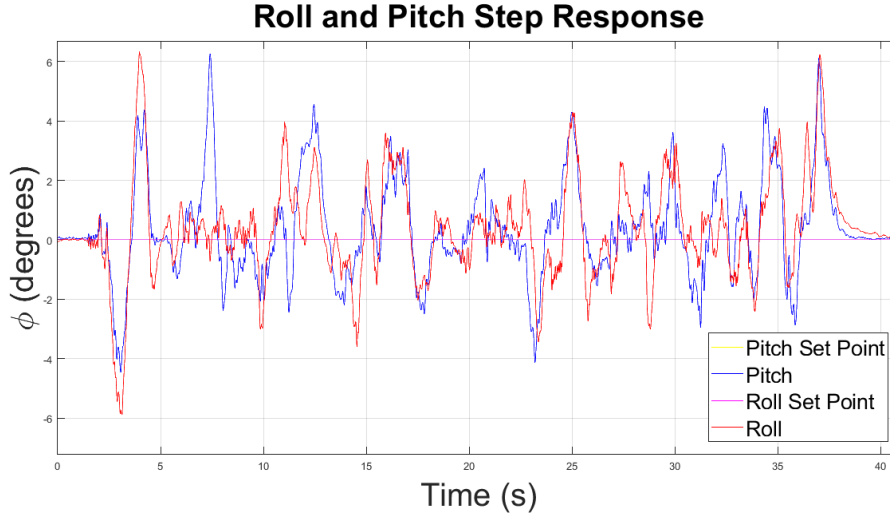


Figure 5.26: Self-Leveling in Indoor Test

5.4.2 Outdoor Tests

The outdoor test was carried out twice, uphill and then downhill. Figures 5.27 and 5.28 show the tests respectively, and the table 5.4 the errors of the test.

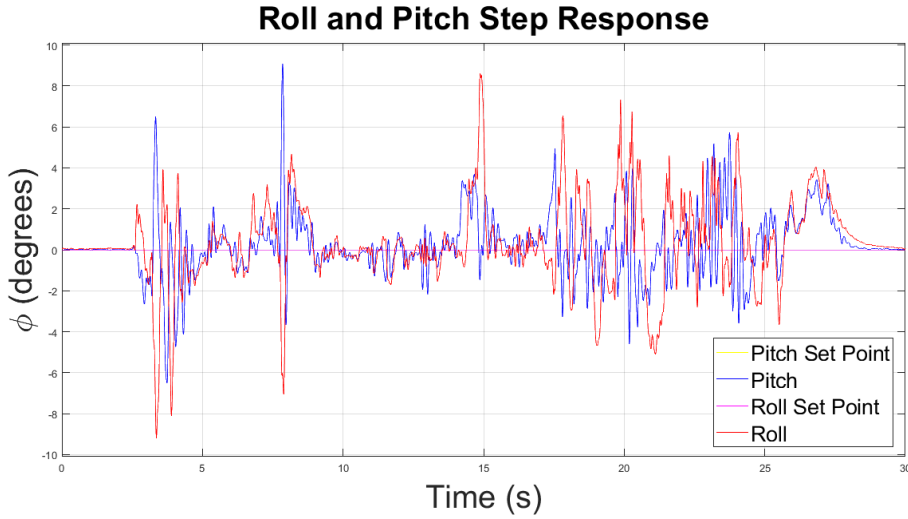


Figure 5.27: First Outdoor Test

The errors from both tests don't show a big difference between the vehicle going uphill or downhill, and unlike the indoor test, the largest angle in the module is close to 10 degrees.

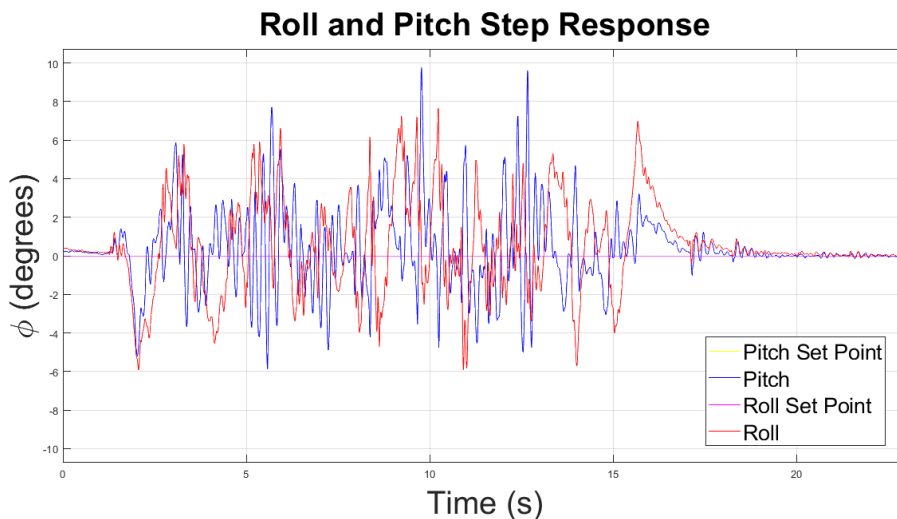


Figure 5.28: Second Outdoor Test

	Pitch	Roll
ME Uphill	-0.2351	-0.3367
RMSE Uphill	1.5393	2.0696
ME Downhill	-0.3569	-0.4930
RMSE Downhill	1.9622	2.3117

Table 5.4: Outdoor Test Errors

5.4.3 Take off and Landing Operations of an drone

In this test, the vehicle was stationary with the platform on it, and finally on the platform a drone that performed the take-off and landing operations on the platform, Figure 5.29 shows the response of the platform sensor and table 5.5 shows the errors related to this test.

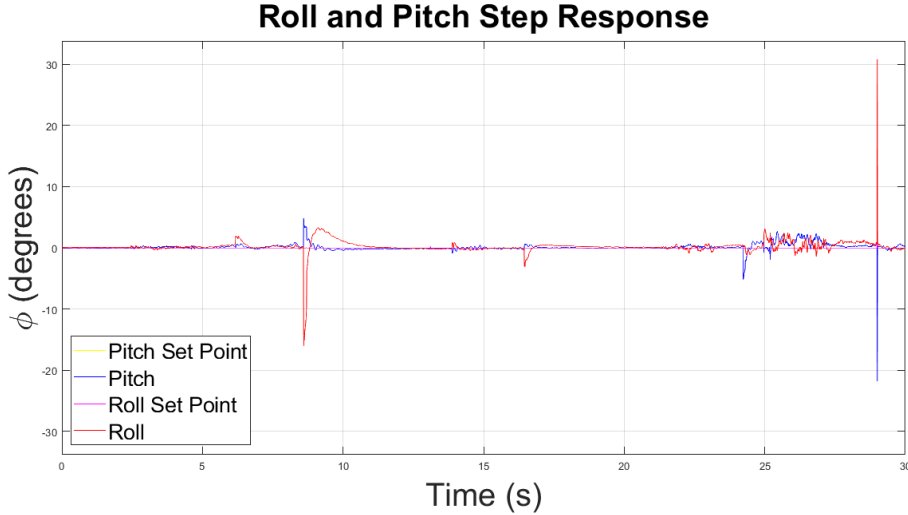


Figure 5.29: drone landing

	Pitch	Roll
ME	-0.1196	-0.2042
RMSE	0.5607	1.1894

Table 5.5: Indoor Test Errors

The graph shows peaks in the angles at take-off and landing, but the drone used is small and light, incapable of unleveling the platform as shown by the peaks. These outliers are due to the fact that the sensor measures acceleration in all 3 axes, so when the drone took off or landed it generated a peak of acceleration with the small impact, and this acceleration was taken into account when calculating the pitch and roll angles.

Chapter 6

Conclusion and Future Work

With the results obtained in the previous chapter 5, the tests and evaluation of the platform kinematics proved to be sufficient for applications in outdoor environments, since the platform's amplitude can measure and travel more than 30 degrees. Although the amplitude meets the objectives, unfortunately the angles of interest for each axis do not reach 15° for pitch and -15° for roll, due to errors in the platform assembly.

The structure has a area of 500x500 mm for UAV landings, which was a good area as the test of 5.4 show. However, it was clear that there is a need to design and build the physical model with special attention, because in order for the platform to follow the calculated kinematics as reliably as possible, it is necessary to have good precision in the physical measurements of the platform and its construction components.

In order to achieve greater precision in the construction, it is important for a designer or mechanic to work together on similar projects.

Another analysis aimed at kinematic measurement is the use of sensors. In this work, the use of a single accelerometer with good filtering has already proven effective with good precision for pitch angle, with 6.55% of error. On the other hand the Roll angle has 15.30% of error without offset correction, and 10.57% of error considering the offset equals to mean error. However, as the scalability of this work becomes greater, there is the question of using a gyroscope or more accelerometers using the sensor fusion technique to better filter the platform inclination data.

Regarding the control of the motors to adjust the pitch and roll angles, it was seen from the results and graphs in the section 5 that a P controller with low gain already stabilizes the system with a good step response, having a low error in steady state, low overshoot and low rise time.

Aiming for a platform that can carry various types of UAV, in general hexacopters or professional drones tend to be heavier than 3kg, in the case of this platform it can stabilize loads of up to 4kg, for use with small UAV this platform already satisfies the problem in outdoor environments with inclination of up to 25%. However, cooperation with professional UAVs such as hexacopters will require better mechanical development so that the dynamics of the platform can carry and stabilize heavier loads, for this reason the development of a platform with another layout such as Delta or Stewart is questioned, in this way it is not necessary to invest in more powerful engines, but it is necessary to use more engines.

With this platform as a tool or module for a mobile robot, the acceleration produced by the vehicle can be measured by the platform if only IMU sensor is used, as seen in the previous Figure 5.29. Therefore, an important point to study is how to measure the pitch and roll angles using another principle in addition to the acceleration on the 3 axes, such as a gyroscope measuring the angular velocity of the 3 axes. Another interesting idea is to use another IMU, placing one on the platform and the other on the vehicle, so that the acceleration signal measured by the movement of the vehicle can be removed from the platform sensor, leaving only the acceleration due to the earth's gravity.

Bibliography

- [1] G. S. Berger, M. Teixeira, A. Cantieri, *et al.*, “Cooperative heterogeneous robots for autonomous insects trap monitoring system in a precision agriculture scenario,” *Agriculture (Switzerland)*, vol. 13, 2 Feb. 2023, ISSN: 20770472. DOI: 10.3390/agriculture13020239.
- [2] A. Atefi, Y. Ge, S. Pitla, and J. Schnable, *Robotic technologies for high-throughput plant phenotyping: Contemporary reviews and future perspectives*, Jun. 2021. DOI: 10.3389/fpls.2021.611940.
- [3] C. Zhang, B. Zhang, and H. Zhang, “Design of automatic picking robot based on 2-dof stabilized platform,” Institute of Electrical and Electronics Engineers Inc., Aug. 2021, pp. 1152–1157, ISBN: 9781665441001. DOI: 10.1109/ICMA52036.2021.9512645.
- [4] K. G. Fue, W. M. Porter, E. M. Barnes, and G. C. Rains, *An extensive review of mobile agricultural robotics for field operations: Focus on cotton harvesting*, Mar. 2020. DOI: 10.3390/agriengineering2010010.
- [5] G. G. de Castro, T. M. Santos, F. A. Andrade, *et al.*, “Heterogeneous multi-robot collaboration for coverage path planning in partially known dynamic environments,” *Machines*, vol. 12, 3 Mar. 2024, ISSN: 20751702. DOI: 10.3390/machines12030200.
- [6] Y. Wu, S. Wu, and X. Hu, “Cooperative path planning of uavs ugvs for a persistent surveillance task in urban environments,” *IEEE Internet of Things Journal*, vol. 8, pp. 4906–4919, 6 Mar. 2021, ISSN: 23274662. DOI: 10.1109/JIOT.2020.3030240.

- [7] M. Stampa, U. Jahn, D. Fruhner, T. Streckert, and C. Rohrig, “Scenario and system concept for a firefighting uav-ugv team,” Institute of Electrical and Electronics Engineers Inc., 2022, pp. 253–256, ISBN: 9781665472609. DOI: 10.1109/IRC55401.2022.00049.
- [8] S. M. Nogar, “Autonomous landing of a uav on a moving ground vehicle in a gps denied environment,” in *2020 IEEE International Symposium on Safety, Security, and Rescue Robotics (SSRR)*, 2020, pp. 77–83. DOI: 10.1109/SSRR50563.2020.9292607.
- [9] F. S. Dalang, G. Kulathunga, and R. Khusainov, “Autonomous landing of an unmanned aerial vehicle on a mobile platform,” Institute of Electrical and Electronics Engineers Inc., 2023, pp. 151–156. DOI: 10.1109/ICACR59381.2023.10314602.
- [10] S. W. Sim, B. H. Kwan, W. S. Yap, and D. W. K. Ng, “Development of an autonomous mobile manipulator for pick and place operation using 3d point cloud,” Institute of Electrical and Electronics Engineers Inc., 2022, pp. 280–285, ISBN: 9781665470988. DOI: 10.1109/ICSPC55597.2022.10001817.
- [11] P. Anggraeni, I. Rokhim, and R. M. Salam, “Design and development of multiple mobile manipulator robots using gazebo-ros,” Institute of Electrical and Electronics Engineers Inc., 2020, pp. 672–676, ISBN: 9781728195674. DOI: 10.1109/iCAST51016.2020.9557660.
- [12] C. G. Grlj, N. Krznar, and M. Pranjić, *A decade of uav docking stations: A brief overview of mobile and fixed landing platforms*, Jan. 2022. DOI: 10.3390/drones6010017.
- [13] BearingNews, *Nsk developing outdoor mobile robot platform for smooth and gentle transport of objects*, <https://www.bearing-news.com/nsk-developing-outdoor-mobile-robot-platform-smooth-and-gentle-transport-of-objects/>, Accessed on May 13, 2024.
- [14] Topographic-map, *Mapa topográfico península ibérica*, <https://pt-pt.topographic-map.com/map-hfq18/Península-Ibérica/>, Accessed on may 13, 2024.

- [15] J. D. Sánchez-Martínez and A. P. Cabrera, *The olive monoculture in the south of spain*, 2015. [Online]. Available: <http://www.ujaen.esjdsanche@ujaen.es> <http://www.ujaen.esapaniza@ujaen.es>.
- [16] A. J. de Jesus Gonçalves, *El valor funcional de la estructura verde urbana - aportación desde el estudio de los espacios verdes de la ciudad de bragança (portugal)*, 2013.
- [17] Forest GIS. “Declividade: Como converter de graus para porcento e vice-versa.” Accessed: August 2, 2024. (May 2021), [Online]. Available: <https://forest-gis.com/2021/05/declividade-como-converter-de-graus-para-porcento-e-vice-versa.html>.
- [18] S. Sarma, R. Parasuraman, and R. Pidaparti, “Impact of heterogeneity in multi-robot systems on collective behaviors studied using a search and rescue problem,” in *2020 IEEE International Symposium on Safety, Security, and Rescue Robotics, SSRR 2020*, Institute of Electrical and Electronics Engineers Inc., Nov. 2020, pp. 290–297, ISBN: 9781665403900. DOI: [10.1109/SSRR50563.2020.9292588](https://doi.org/10.1109/SSRR50563.2020.9292588).
- [19] K. Dalamagkidis, S. Ioannou, K. Valavanis, and E. Stefanakos, “A mobile landing platform for miniature vertical take-off and landing vehicles,” in *2006 14th Mediterranean Conference on Control and Automation*, 2006, pp. 1–6. DOI: [10.1109/MED.2006.328767](https://doi.org/10.1109/MED.2006.328767).
- [20] Y. Feng, H. Wang, J. Wu, H. Song, and I.-M. Chen, “Design of a novel self-balancing mechanism on agv for stable stair climbing,” in *IECON 2020 The 46th Annual Conference of the IEEE Industrial Electronics Society*, 2020, pp. 594–599. DOI: [10.1109/IECON43393.2020.9255033](https://doi.org/10.1109/IECON43393.2020.9255033).
- [21] Wikipedia contributors, *Aircraft principal axes — Wikipedia, the free encyclopedia*, https://en.wikipedia.org/w/index.php?title=Aircraft_principal_axes&oldid=1239538537, [Online; accessed 12-August-2024], 2024.

- [22] “Sensors to detect motion in three dimensions.” Accessed: August 2, 2024, TOKYO AIRCRAFT INSTRUMENT CO., LTD. (), [Online]. Available: <https://www.tkk-air.co.jp/english/aerospace/inertial-sensors.html>.
- [23] Wikipedia contributors, *Rotation matrix — Wikipedia, the free encyclopedia*, [Online; accessed 14-August-2024], 2024. [Online]. Available: https://en.wikipedia.org/w/index.php?title=Rotation_matrix&oldid=1237822022.
- [24] M. M. Kopichev, A. V. Putov, and A. N. Pashenko, “Ball on the plate balancing control system,” vol. 638, Institute of Physics Publishing, Oct. 2019. DOI: 10.1088/1757-899X/638/1/012004.
- [25] E. K. Kaneda, G. Berger, V. H. Pinto, *et al.*, *Developement an platform with 2 dof to assist the cooperation between grounded mobile robots and uavs in landing operations*.
- [26] Wikipedia contributors, *Reymond clavel — Wikipedia, the free encyclopedia*, [Online; accessed 27-August-2024], 2023. [Online]. Available: https://en.wikipedia.org/w/index.php?title=Reymond_Clavel&oldid=1158375329.
- [27] Wikipedia contributors, *Delta robot — Wikipedia, the free encyclopedia*, [Online; accessed 27-August-2024], 2024. [Online]. Available: https://en.wikipedia.org/w/index.php?title=Delta_robot&oldid=1237706245.
- [28] R. W. II, *The delta parallel robot: Kinematics solutions*, <http://www.ohio.edu/people/williar4/html/pdf/DeltaKin.pdf>, Internet Publication, Accessed: January 2016, 2016.
- [29] B. Siciliano and O. Khatib, *Springer Handbook of Robotics*. Springer, 2016, ISBN: 978-3319325507.
- [30] M. Alkhedher, T. Younes, O. Mohamad, and U. Ali, “Adaptive 6 dof self-balancing platform for autonomous vehicles,” *International Journal of Computing and Digital Systems*, Jan. 2020.

- [31] BotnRoll, *Motor 12v dc com encoder 157rpm*, <https://www.botnroll.com/pt/motores-dc/3411-motor-12v-dc-com-encoder-157rpm.html>, Accessed: 2024-05-13, 2024.
- [32] Wikipédia, *Servomotor — wikipédia, a encyclopédia livre*, [Online; accessed 11-março-2024], 2024. [Online]. Available: <https://pt.wikipedia.org/w/index.php?title=Servomotor&oldid=67609568>.
- [33] Dejan. “How to control servo motors with arduino – complete guide.” Accessed: January 6, 2025. (), [Online]. Available: https://howtomechatronics.com/how-it-works/how-servo-motors-work-how-to-control-servos-using-arduino/?utm_content=cmp-true.
- [34] C. Fiore, *Stepper motors basics: Types, uses, and working principles*, 2023.
- [35] LINAK, *How do linear actuators work?* Accessed: 2024-09-25, 2024. [Online]. Available: <https://www.linak.com/products/linear-actuators/#/how-do-linear-actuators-work>.
- [36] BotnRoll, *Motor linear 12vdc c/100mm de curso 7mm/s 750n*, <https://www.botnroll.com/pt/motores-dc/3582-motor-linear-12vdc-c-100m-de-curso-7mm-s-750n.html>, Accessed: 2024-05-13, 2024.
- [37] H. Guo and M. Uradzinski, “The usability of mti imu sensor data in pdr indoor positioning,” in *2018 25th Saint Petersburg International Conference on Integrated Navigation Systems (ICINS)*, 2018, pp. 1–4. doi: 10.23919/ICINS.2018.8405864.
- [38] H. M. Saputra, T. Permadi, C. H. A. Baskoro, N. S. M. Nor, B. Abdussalam, and M. Y. Rezaldi, “Effect of imu sensor positioning on 1-dof angle measurement accuracy for robotic charging station (rocharg-v1) manipulator,” in *2023 International Conference on Computer, Control, Informatics and its Applications (IC3INA)*, 2023, pp. 96–101. doi: 10.1109/IC3INA60834.2023.10285798.

- [39] F. Ge, D. Liu, L. Lin, Z. Yang, and G. Yan, “Fast self-resonant startup procedure for digital mems gyroscope system,” in *2012 7th IEEE International Conference on Nano/Micro Engineered and Molecular Systems (NEMS)*, 2012, pp. 669–672. DOI: 10.1109/NEMS.2012.6196864.
- [40] Y. Sun, F. Li, Y. Chen, and X. Xu, “A magnetic vector aided calibration method for mems gyroscope,” in *2021 IEEE International Conference on Unmanned Systems (ICUS)*, 2021, pp. 26–31. DOI: 10.1109/ICUS52573.2021.9641307.
- [41] W. A. Gill, I. Howard, I. Mazhar, and K. McKee, “A review of mems vibrating gyroscopes and their reliability issues in harsh environments,” *Sensors*, vol. 22, no. 19, 2022, ISSN: 1424-8220. DOI: 10.3390/s22197405. [Online]. Available: <https://www.mdpi.com/1424-8220/22/19/7405>.
- [42] L. Yang, Z. Rong, Z. Bin, and G. Zhenyi, “Design of soc for special measurement and control of mems gyroscope based on arm cortex-m3,” in *2019 IEEE International Conference on Power, Intelligent Computing and Systems (ICPICS)*, 2019, pp. 296–299. DOI: 10.1109/ICPICS47731.2019.8942558.
- [43] Y. Yu, B. Chen, J. Tao, *et al.*, “A novel high sensitivity mems acoustic gyroscope by measuring phase shift,” in *2015 IEEE SENSORS*, 2015, pp. 1–4. DOI: 10.1109/ICSENS.2015.7370329.
- [44] Wikipédia, *Força inercial de coriolis — wikipédia, a encyclopédia livre*, [Online; accessed 29-dezembro-2023], 2023. [Online]. Available: https://pt.wikipedia.org/w/index.php?title=For%C3%A7a_inercial_de_Coriolis&oldid=67202209.
- [45] Arduino, *Arduino Uno Rev3 Documentation*, Accessed: 2024-10-08, 2024. [Online]. Available: <https://docs.arduino.cc/hardware/uno-rev3/>.
- [46] Espressif Systems, *ESP-IDF Documentation: ESP32 Hardware Reference V5.2*, Accessed: 2024-10-08, 2024. [Online]. Available: <https://docs.espressif.com/projects/esp-idf/en/latest/esp32/hw-reference/index.html>.

- [47] Microchip Technology Inc., *Microchip Microcontrollers and Microprocessors*, Accessed: 2024-10-08, 2024. [Online]. Available: <https://www.microchip.com/en-us/products/microcontrollers-and-microprocessors>.
- [48] STMicroelectronics, *ARM 32-bit Microcontrollers*, Accessed: 2024-10-08, 2024. [Online]. Available: https://www.st.com/content/st_com/en/arm-32-bit-microcontrollers.html.
- [49] Raspberry Pi Foundation, *Raspberry Pi Datasheets*, Accessed: 2024-10-08, 2024. [Online]. Available: https://datasheets.raspberrypi.com/?_gl=1*gbghpp*_ga*Nzc4ODkyMTA1LjE3MzA3MTgwMTg.*_ga_22FD70LWDS*MTczMDcxODAxNy4xLjEuMTczMDcxODAyMi4..
- [50] N. S. Nise, *CONTROL SYSTEMS ENGINEERING*, 7th ed. WILEY, 2014, ISBN: 978-1-118-80082-9.
- [51] M. T. Inc. “Discrete pid controller on tinyavr and megaavr - application note avr221.” Accessed: January 6, 2025. (2016), [Online]. Available: https://ww1.microchip.com/downloads/aemDocuments/documents/OTH/ApplicationNotes/ApplicationNotes/Atmel-2558-Discrete-PID-Controller-on-tinyAVR-and-megaAVR_ApplicationNote_AVR221.pdf.
- [52] Wikipedia contributors, *Proportional–integral–derivative controller — Wikipedia, the free encyclopedia*, [Online; accessed 9-October-2024], 2024. [Online]. Available: https://en.wikipedia.org/w/index.php?title=Proportional%E2%80%93integral%E2%80%93derivative_controller&oldid=1250109285.
- [53] F. Neves. “Controlador pid digital: Uma modelagem prática para microcontroladores – parte 1.” Accessed: January 6, 2025. (May 2014), [Online]. Available: <https://embarcados.com.br/controlador-pid-digital-parte-1/>.
- [54] R. Dalmaso and F. Martins, “Projeto e desenvolvimento de uma interface flexível de entrada/saída via usb para automação de processos,” Jan. 2010. DOI: 10.13140/2.1.1763.6482.

- [55] K. Curtis and M. T. Inc., *Pid fan speed control for 4-wire fans*, Accessed: January 6, 2025, 2020. [Online]. Available: <https://ww1.microchip.com/downloads/aemDocuments/documents/MCU08/ApplicationNotes/ApplicationNotes/PID-Fan-Speed-Control-for-4-Wire-Fans-00003530A.pdf>.
- [56] Texas Instruments, *DRV8825 Stepper Motor Driver IC*, Accessed: 2024-10-08, 2010. [Online]. Available: <https://www.ti.com/lit/ds/symlink/drv8825.pdf?ts=1730875803946>.
- [57] Joy-It, *NEMA17-06 Stepper Motor Datasheet*, Accessed: 2024-10-08, 2022. [Online]. Available: https://joy-it.net/files/files/Produkte/NEMA17-06/NEMA17-06_Datasheet.pdf.
- [58] tyeth, *Adafruit adxl345 library*, https://github.com/adafruit/Adafruit_ADXL345, Accessed: 2024-08-02, Nov. 2023.

Appendix A

Proposta Original do Projeto



**Proposta de tema para
Dissertação/Estágio/Projeto - Trabalho de Conclusão de Curso**

Orientador da Instituição onde se realiza o trabalho:

José Lima	jllima@ipb.pt
-----------	---------------

Instituição do orientador:

IPB	ESTIG
-----	-------

Co-orientador da Instituição parceira:

Flávio Luiz Rossini	frossini@utfpr.edu.br
---------------------	-----------------------

Instituição do co-orientador:

UTFPR	DAELN
-------	-------

Curso ou cursos da Instituição do orientador onde se propõe que o trabalho seja realizado:

Mestrado em Engenharia Eletrotécnica e de Computadores
--

Título do trabalho:

Two-degree-of-freedom platform as a tool for cooperation between mobile robot and UAVs
--

Palavras chave:

Robótica, Controle, Plataforma Autonivelante, cooperação.

Objetivos:

O principal objetivo desta dissertação consiste no estudo do comportamento cinemático de uma plataforma autonivelante dedicada a operações cooperativas entre sistemas robóticos heterogêneos. Neste sentido, tanto o desenvolvimento do sistema de controle quanto de hardware será desenvolvido e validado em ambientes diversos, tais como terrenos regulares e irregulares.

Descrição adicional:

Umaned ground Veichles (UGVs) e Unmanned Aerial Veichles (UAVs) representam uma grande relevância no atual contexto tecnológico, possibilitando sua aplicação em diferentes áreas de conhecimento. A abordagem deverá ser desenvolvida e aplicada a operações por UAVs de pequeno porte, seja ele aplicado em ambiente interno ou externo. Durante a dissertação deverá ser construído um protótipo de plataforma auto-nivelante que permita aterrissar um drone na superfície horizontal independentemente do ângulo do seu suporte.

Metodologia/Plano de trabalhos:

Mês 1 e 2 - Estudo sobre o Estado da Arte vinculado aos principais métodos e técnicas dedicados ao controle e desenvolvimento de plataformas autonivelantes.
Mês 3, 4 e 5 - Desenvolvimento da plataforma autonivelante e de modelos de controle.
Mês 6- Implementação de modelos cinematográficos e de controle.
Mês 7 - Testes e validação do sistema em ambiente virtual e real.
Mês 8 e 9 - Escrita da dissertação e de um artigo científico a submeter a conferência na área.

Recursos necessários:

Materiais do almoxarifado do IPB
Impressões 3D

Appendix B

Outro(s) Apêndice(s)

GitHub repository: <https://github.com/Kanedinha>.